Understanding and leveraging phenotypic plasticity during metastasis formation

Saumil Shah[1,*], Lisa-Marie Philipp[2], Susanne Sebens[2], Arne Traulsen[1], Michael Raatz[1]

[1]Department of Evolutionary Theory, Max Planck Institute for Evolutionary Biology, Ploen, August-Thienemann-Str. 2, 24306 Ploen
[2]Institute for Experimental Cancer Research, Kiel University and University Hospital Schleswig-Holstein, Campus Kiel, Arnold-Heller-Str. 3, Building U30, Entrance 1, 24105 Kiel
*shah{at}evolbio.mpg.de

Abstract

Cancer metastasis is the primary cause of poor prognosis and cancer-related fatalities. Metastasis formation has long been identified as a process of the detrimental systemic spread of cancer, yet cure remains a challenge. Successful metastasis formation requires tumor cells to be proliferative and invasive; however, cells cannot be effective at both tasks at the same time. Tumor cells compensate for this trade-off by changing their phenotype during metastasis formation through phenotypic plasticity. Phenotypic plasticity is a cell's ability to adopt different phenotypes stochastically or driven by environmental cues. Given the different selection pressures and competitive interactions that tumor cells face in their microenvironment, it is poorly understood how plasticity shapes the process of metastasis formation. Here, we develop an ecology-inspired mathematical model that captures stochastic phenotypic plasticity and accounts for resource competition between phenotypes. We find that phenotypically plastic tumor cell populations can drive cancer metastasis. Additionally, these populations have a stable phenotype equilibrium that maintains tumor cell heterogeneity. By modeling treatment types inspired from chemo- and immunotherapy, we also highlight that phenotypically plastic populations are protected against interventions. Turning this strength into a weakness, we corroborate current clinical practices to use this plasticity as a target for adjuvant therapy. By providing a quantitative description of a phenotypically plastic cell population and its response to interventions, we can thus achieve a better mechanistic understanding of tumor cell biology and its consequences for metastasis formation.

1 Introduction

Cancer metastasis formation, or the spread and growth of tumor cells throughout the body, is the cause of more than 60% of cancer-related deaths (Dillekås et al., 2019). Despite many decades of drug development for cancer, the survival rate for patients with metastatic cancer remains low (Siegel et al., 2020; Sung et al., 2021). The process of metastasis is a multistage process that includes local invasion by the tumor cells, invading into the circulatory system, survival in circulation, arrest at a distant tissue, getting out of the circulation, survival, adaptation and outgrowth in a new environment (Gupta and Massagué, 2006; Weinberg, 2014; Turajlic and Swanton, 2016). Tumor cells face selection for proliferation, locally at each site of cancer, and for invasiveness and motility during the spread between two sites. These changing selection pressures during metastasis are driven by environmental factors and interactions with different surroundings (Shlyakhtina et al., 2021; Group Young Researchers in Inflammatory Carcinogenesis et al., 2021).

How tumor cells respond to these frequently changing environmental conditions is crucial for their persistence. Tumor cell populations possess several adaptive strategies to cope with such fluctuating environments. A subset of these strategies relies on diversity-generating mechanisms. In addition to genetic mechanisms, such as mutations, copy number alterations, and translocations, there are non-genetic mechanisms to generate diversity, such as epigenetic regulation, stochastic gene expression, and cellular differentiation hierarchies (Caiado et al., 2016; Shlyakhtina et al., 2021). All these factors are internal to the cell. In addition, the local environment can be substantial; local variations in the tumor microenvironment may generate functional heterogeneity among clonal tumor cells (Shlyakhtina et al., 2021; Group Young Researchers in Inflammatory Carcinogenesis et al., 2021). An early review by West-Eberhard (1989) emphasizes plasticity as a diversity-generating mechanism and its contribution to altering traits. Plasticity also affects population and eco-evolutionary dynamics (Fischer et al., 2014).

One prominent outcome of epithelial tumor cell plasticity is the range of phenotypes and transitions on the spectrum from epithelium to mesenchyme. Epithelial cells are proliferative but cannot move, while mesenchymal cells are motile and invasive but proliferate slowly (Giese et al., 1996). Both proliferative and invasive phenotypes are crucial for tumor progression and metastasis. Thus, shifts in the phenotype of tumor cells by epithelial-mesenchymal plasticity are thought to be indispensable for cancer metastasis (Zheng et al., 2015; Jolly et al., 2017, 2018; Hong et al., 2018). Consequently, during the epithelial-to-mesenchymal transition, partial mesenchymal features are gained, and epithelial features are progressively lost, leading to altered surface marker expression, decreased cell-cell adhesion, and motility-facilitating cytoskeleton reorganization (Dongre and Weinberg, 2019). The reverse happens during the mesenchymal-to-epithelial transition. The plasticity between epithelial and mesenchymal phenotypes was found to be promoted by interactions with the tumor microenvironment. Among others, high levels of Transforming Growth Factor β (TGF-β) are critical drivers toward more mesenchymal phenotypes (Nieto et al., 2016; Dongre and Weinberg, 2019; Group Young Researchers in Inflammatory Carcinogenesis et al., 2021).

Different treatment types can select differently on this plasticity (Raatz et al., 2021). The current first-line treatment for many cancers is chemotherapy which targets cell proliferation. A more recent treatment option for some cancers is immunotherapy which comprises antibody-based or cellular therapies targeting molecules present on the cell membrane of the cancer cells. These differential selection pressures suggest classifying treatments into growth-dependent or growth-independent treatments. As epithelial-like phenotypes proliferate faster, they are more sensitive to chemotherapy than mesenchymal phenotypes. Immunotherapy should target all phenotypes similarly, assuming that it does not target surface markers that change during epithelial-mesenchymal transition. Adjuvant therapies, such as TGF-β blockers, are promising candidates to modify the transition process and, thus, ultimately, the phenotypic plasticity of tumor cells (Liu et al., 2012; Pickup et al., 2013; Lee et al., 2022).

Mathematical modeling presents an invaluable approach to understanding the mechanisms and consequences of genetic and non-genetic diversity-generating mechanisms. Along this line, Zhou et al. (2019) modeled the hierarchical cellular diversity created by differentiation and de-differentiation, with stem cells at the root of the hierarchy and specialized cells at its leaves. Gupta et al. (2011) and Li and Thirumalai (2022) showed with experiments and mathematical modeling that phenotypically plastic breast cancers approach a phenotypic equilibrium and can maintain phenotypic heterogeneity. A mathematical model of phenotype switching between drug-sensitive and drug-resistant cells in non-small cell lung cancer (Cassidy et al., 2021) also shows similar behavior. Such plastic mechanisms in tumor cells cause reduced efficacy of chemotherapy and acquired therapeutic resistance (Zheng et al., 2015; Ma et al., 2020; Esposito et al., 2021). In a spatial, multi-organ model, Franssen and Chaplain focus specifically on epithelial-mesenchymal transitions during metastasic spread without treatment (Franssen and Chaplain, 2020). In a recent paper, we modeled the phenotype switching between fast and slow proliferating B cells during the relapse dynamics in acute lymphoblastic leukemia and investigated the impacts of treatment on phenotypic heterogeneity (Raatz et al., 2021).

In this paper, we investigate i) how different characteristics of plasticity shape the phenotype distribution, ii) how this distribution determines the transition dynamics between epithelial and mesenchymal phenotypes at primary and secondary tumor sites, and iii) how these dynamics are affected by chemo- or immunotherapy, particularly applied as adjuvant therapy (after surgical reduction of the primary tumor mass), and additionally by a tumor-phenotype-modifying therapy.

2 Methods

We investigate the onset of metastasis formation mediated by the plasticity between epithelial and mesenchymal phenotypes. We use an ecology-inspired approach to identify tumor phenotypes with species in an ecosystem, drawing on the usefulness of ecological concepts for understanding cancer biology (Basanta and Anderson, 2013; Korolev et al., 2014). We use the competitive Lotka-Volterra system (Smale, 1976; Hofbauer and Sigmund, 1998) with additional terms that capture transitions between phenotypes. We go beyond earlier approaches that featured two cell types (Cassidy et al., 2021; Li and Thirumalai, 2022) and account for the recently established

prominence of hybrid phenotypes characterized by both partial epithelial and mesenchymal markers (Jolly et al., 2018). This results in a multi-compartment model similar to those presented in Zhou et al. (2019) and Raatz et al. (2021), but with added competition and more flexibility in specifying the transition process. Using this model, we examine the epithelial-mesenchymal plasticity and characterize how different properties of the plastic transition shape the resulting tumor heterogeneity.

Model

We represent the phenotypic heterogeneity as a collection of N different tumor phenotypes at different sites of cancer (Fig. 1). These phenotypes range from the most epithelial phenotype, E, over $N-2$ hybrid phenotypes H, to the most mesenchymal phenotype, M. We assume that all tumor phenotypes share resources at a given cancer site and that the tumor population follows logistic growth. Additionally, we assume that the tumor cells are phenotypically plastic, i.e., they can change to an adjacent, more epithelial-like, or mesenchymal-like phenotype in bidirectional phenotype transitions.

We track the phenotype abundance x_i over time for each tumor phenotype i, $i = 1, 2, \ldots, N$. Each cell of tumor phenotype i grows intrinsically at rate r_i. The cells switch to the next functionally more mesenchymal phenotype, $i \to i+1$, at rate T_{EM}, and to the next functionally more epithelial type, $i \to i-1$, at rate T_{ME}. Resource scarcity in the microenvironment induces a density-dependent, logistic competition captured by $r_i \frac{M}{K}$, where $M = \sum_{i=1}^{N} x_i$ is the total population abundance and K is the carrying capacity. We assume that all phenotypes are equally competitive for resources, i.e., the competition term is equal for all phenotypes. Relaxing this assumption qualitatively does not affect our results and is explored in the supplementary text (Section 5.3.1)

Further, we assume linearly decreasing growth rates from epithelial to mesenchymal phenotypes, reflecting the higher proliferation rates of epithelial cells. We scale all growth rates relative to the epithelial growth rate r_1, and express the growth rate for the ith phenotype as $r_i = r_1 - (r_1 - r_N)\,\frac{i-1}{N-1}$. We will show that the particular choice of the growth rate decline does not affect our results qualitatively. We assume that the transition rates are equal for all phenotypes and scaled to the epithelial growth rate r_1 with a constant c, $0 \leq c < \infty$. Thus, transitions faster than proliferation, $c > 1$, can be interpreted as within-generational phenotype plasticity, e.g. altered patterns of posttranscriptional regulation, and transitions slower than proliferation $c < 1$ can be attributed to transgenerational plasticity, such as epigenetic changes. We explore the effect of growth rate-dependent transition rates in the supplementary text (Section 5.3.2). To account for a potential bias in the direction of plastic transitions, we introduce the transition bias λ, $-1 \leq \lambda \leq 1$, which determines the probability of a cell switching to the adjacent epithelial or mesenchymal phenotype. A positive transition bias $\lambda > 0$ implies a bias towards becoming more mesenchymal, $\lambda < 0$ results in a higher probability of switching to a more epithelial phenotype. With these presumptions, the transition rates become $T_{EM} = c\,(1+\lambda)\,r_1$ and $T_{ME} = c\,(1-\lambda)\,r_1$. The parameters of our model are given in Table 1.

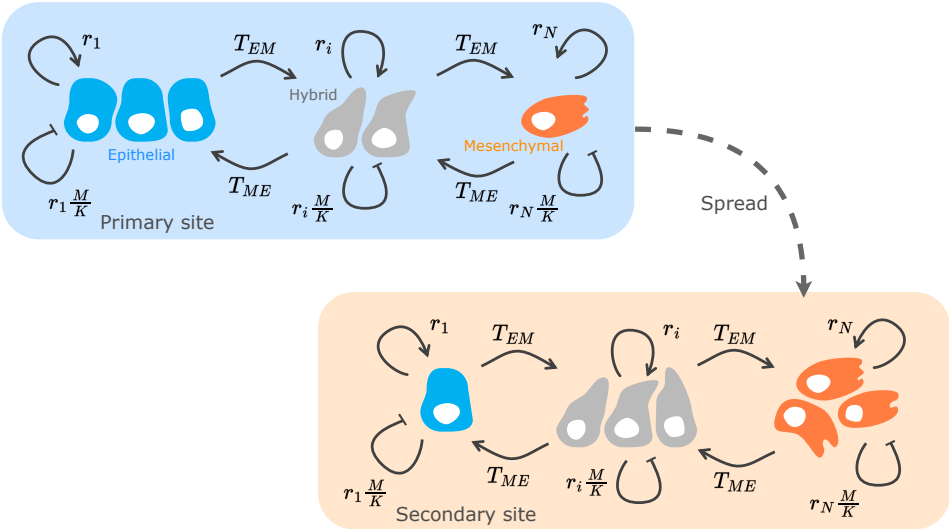

Figure 1: **Model structure capturing phenotypic heterogeneity at the primary and secondary tumor site.** We focus on the competitive growth of heterogeneous tumor cell populations at each tumor site. The dashed arrow represents the not explicitly specified spread of cancer cells between the primary and secondary sites. The different compartments in the model represent epithelial, hybrid, and mesenchymal phenotypes at a site. The solid arrows indicate competitive growth and transitions in phenotype. Phenotype i grows at rate r_i and transitions to the adjacent more mesenchymal-like type at rate T_{EM} and to the adjacent more epithelial-like type at rate T_{ME}. Resource competition is modeled with the term $r_i \frac{M}{K}$ where $M = \sum_{i=1}^{N} x_i$ is the total population abundance, and K is the carrying capacity. The epithelial phenotype can only transition to the more mesenchymal-like adjacent hybrid phenotype, and the mesenchymal phenotype can only transition to the epithelial-like adjacent hybrid phenotype; thus, the epithelial and mesenchymal phenotypes are the terminal phenotypes. Here, we show only one hybrid phenotype, but we also investigate the effect of a larger number of hybrid phenotypes.

Treatment types and schemes

To investigate the effect of drug treatment on phenotypically plastic tumor cell populations, we apply two different treatment types. The mortality exerted on the cells of a particular phenotype by the two treatment types either does or does not depend on the phenotype's growth rate. The death rate exerted by growth-dependent treatment is $m_D r_i$, and the death rate by growth-independent treatments is m_I. We chose m_I such that the reduction of tumor cell abundance at the end of the treatment duration is identical for both treatment types. To find m_I, we use $c = 1$, $\lambda = 0$, $m_D = 1$. Throughout this study, treatment is always applied for a fixed duration of 10 time units.

These assumptions result in a system of ordinary differential equations describing the change

Symbol	Description	Value
x_i	abundance of ith tumor phenotype	
M	sum of all phenotype abundances	$\sum_{i=1}^{N} x_i$
N	number of tumor phenotypes	3
r_i	growth rate of ith phenotype	$r_1 - (r_1 - r_N)\ \frac{i-1}{N-1}$
r_1	growth rate of epithelial cells	1
r_N	growth rate of mesenchymal cells	$\frac{1}{5}$
K	carrying capacity of a site	1
T_{EM}	transition rate of $i \to i+1$	$c\ (1+\lambda)\ r_1$
T_{ME}	transition rate of $i \to i-1$	$c\ (1-\lambda)\ r_1$
c	transition speed	1
λ	transition bias	0
m_D	growth-dependent treatment intensity	1
m_I	growth-independent treatment intensity	≈ 0.68

Table 1: **Symbols, variables and reference parameters**. Deviations from these values are reported where applicable.

in tumor phenotype abundance,

$$
\begin{aligned}
\frac{dx_1}{dt} &= r_1\ x_1 \left(1 - \frac{M}{K}\right) + c\ r_1\left[(1-\lambda)\ x_2 - (1+\lambda)\ x_1)\right] - (m_D\ r_1 + m_I)\ x_1 \\
&\vdots \\
\frac{dx_i}{dt} &= \underbrace{r_i\ x_i \left(1 - \frac{M}{K}\right)}_{\text{logistic growth}} + \underbrace{c\ r_1\left[(1+\lambda)\ x_{i-1} + (1-\lambda)\ x_{i+1} - 2\ x_i)\right]}_{\text{transitions}} - \underbrace{(m_D\ r_i + m_I)\ x_i}_{\text{treatments}}. \qquad (1) \\
&\vdots \\
\frac{dx_N}{dt} &= r_N\ x_N \left(1 - \frac{M}{K}\right) + c\ r_1\left[(1+\lambda)\ x_{N-1} - (1-\lambda)\ x_N)\right] - (m_D\ r_N + m_I)\ x_N
\end{aligned}
$$

Different drug administration strategies are possible and are of clinical interest. However, in current practice, mostly monotherapies or combined therapies are used, often leading to resistance due to static selection pressures. This motivates us to investigate sequential treatment schemes. The fixed treatment scheme either treats with the same drug throughout the treatment duration or alternates between blocks of different treatment types. The single-block treatment scheme applies either growth-dependent or growth-independent treatment. In the multi-block treatment schemes, we alternate between treatment types and investigate both cases of first treating with growth-dependent or first treating with growth-independent treatment. For the adaptive treatment scheme, at the start of each treatment block, the treatment type is chosen that achieves the higher instantaneous reduction of the whole tumor cell population for the given phenotype

distribution (Raatz et al., 2021). The cancer cell mortality for growth-dependent treatment is $\sum_{i=1}^{N} m_D\, r_i\, x_i$ and the mortality exerted by growth-independent treatment is $\sum_{i=1}^{N} m_I\, x_i$. The comparison of these two terms determines the decision for the treatment type.

Analysis and implementation

We performed linear stability analysis to find the equilibria of Eqs. (1) and their local stability (Strogatz, 2018). The analytical results of this analysis are presented in the Supplementary Text for $N = 2$ and $N = 3$ (Section 5.2), for $N > 3$ stability was confirmed numerically (Fig. S3). Temporal dynamics of the model (Eqs. (1)) were obtained by numerical integration using the `solve_ivp` function from the `Scipy` library (Virtanen et al., 2020) in Python (version 3.9, van Rossum and Drake (2010)). Numpy (Harris et al., 2020) and Matplotlib (Hunter, 2007) were used for computation and plotting. The relevant code can be found at DOI: 10.5281/zenodo.7294563 and the simulation data and figures at DOI: 10.5281/zenodo.7294579.

3 Results

Plastic tumor cell populations have a stable phenotype distribution

Assuming that cells can transition into adjacent epithelial or mesenchymal phenotypes generates a phenotype distribution of abundances along the epithelial-mesenchymal trait axis. Using linear stability analysis (Supplementary text, Section 5.2), we determine the stability and parameter dependence of the equilibria of the phenotype distribution. Without treatment, $m_D = m_I = 0$, the model given by Eqs. (1) has two equilibria. One equilibrium is the state where the tumor vanishes, $x_i = 0$ for $i = 1, 2, \ldots, N$. This equilibrium is unstable, implying that a tumor can always progress and increase in abundance without treatment. The second equilibrium is the state described by

$$x_i^* = K \frac{(1-\lambda)^{N-i}\ (1+\lambda)^{i-1}}{\sum_{j=1}^{N} (1-\lambda)^{N-j}\ (1+\lambda)^{j-1}} \qquad \text{for } i = 1, 2, \ldots, N \tag{2}$$

This equilibrium is stable and describes the coexistence of all phenotypes. The sum of all phenotype abundances at the coexistence equilibrium is K. The stable distribution of phenotypes at the coexistence equilibrium depends on the transition bias λ and the number of phenotypes N. Notably, the stable phenotype distribution does not depend on the growth rate. Thus, only the transitions and not the growth dynamics decide the phenotype abundances at equilibrium, Additionally, this growth independence shows that the particular choice of the decline of growth rates from epithelial to mesenchymal phenotypes does not affect the equilibrium phenotype distribution.

The transition bias controls the stable phenotype distribution

When cells change to a more epithelial or mesenchymal phenotype with the same probability, i.e., when there is no transition bias ($\lambda = 0$), the stable distribution is a uniform distribution (Fig. 2). When there is a transition bias towards the mesenchymal-like phenotype ($\lambda > 0$), there are more mesenchymal-like phenotypes in the stable phenotype distribution, and the mean of the stable

phenotype distribution shifts towards the mesenchymal phenotype (Fig. S1). On the other hand, for a transition bias towards the epithelial-like phenotype ($\lambda < 0$), there are more epithelial-like phenotypes in the stable phenotype distribution, and the mean shifts towards the epithelial phenotype (Fig. 2). The abundance of hybrid phenotypes never exceeds both the epithelial and the mesenchymal phenotypes simultaneously, i.e., the stable phenotype distribution does not have a maximum at hybrid phenotypes.

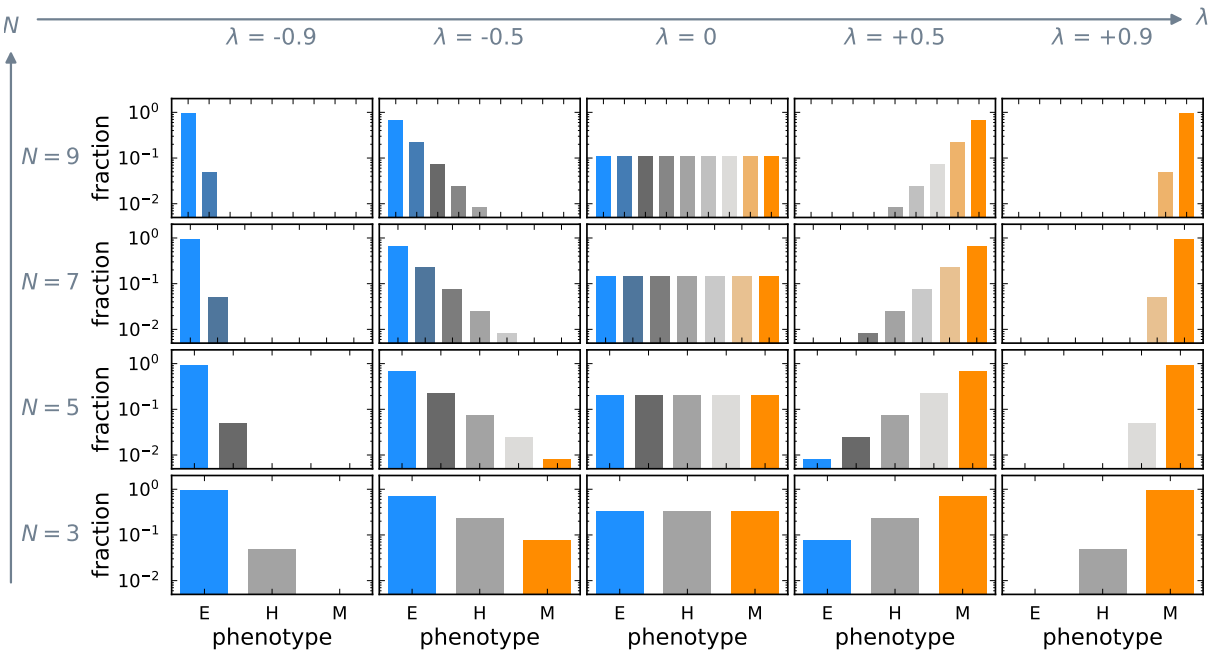

Figure 2: **Phenotype transitions create a stable phenotype distribution**. Each panel shows the distribution of phenotypes (Eq. (2)) relative to the carrying capacity K for a fixed value of the transition bias λ and the number of phenotypes N. The stable phenotype distribution changes with the transition bias λ but remains qualitatively unaffected by changing the number of phenotypes N. The stable distribution is uniform when there is no transition bias to either epithelial or mesenchymal-like phenotypes, i.e., $\lambda = 0$. $\lambda < 0$ introduces a transition bias towards epithelial-like phenotypes and leads to a relative increase in epithelial cells. Conversely, $\lambda > 0$ results in a transition bias towards mesenchymal-like phenotypes and causes a relative increase in mesenchymal cells.

Interestingly, the variance as a proxy for phenotypic heterogeneity of the tumor population is highest when there is no transition bias and $\lambda = 0$ (Fig. S1). The variance decreases and vanishes at the bias extremes $\lambda \to -1$ or $\lambda \to 1$ where transitions become unidirectional. The presence of phenotypes far off the average population phenotype with very low abundances, essential for residual disease in some cancers, is captured by the skewness of the phenotype distribution. We find that skewness is an odd function of the transition bias, vanishing at $\lambda = 0$ and diverging at extreme transition biases (Fig. S1). The number of phenotypes N changes the slopes of mean, variance, and skewness of the stable phenotype distribution as transition bias changes but does not affect their shapes qualitatively (Fig. S1). Accordingly, we will focus on $N = 3$ in the remainder of this study.

The transition speed determines how fast the stable phenotype distribution is approached

While the transition bias λ determines the stable phenotype distribution, the transition speed c affects how fast it is approached. The model (Eqs. (1)) consists of two processes; logistic growth and transitions, where the parameter c scales transitions relative to the growth rate. When transitions are faster than growth, $c > 1$, the population first reaches the stable phenotype distribution and then approaches the carrying capacity. When transitions are slower than growth, $c < 1$, the population first reaches the carrying capacity and then equilibrates to the stable phenotype distribution (Fig. 3).

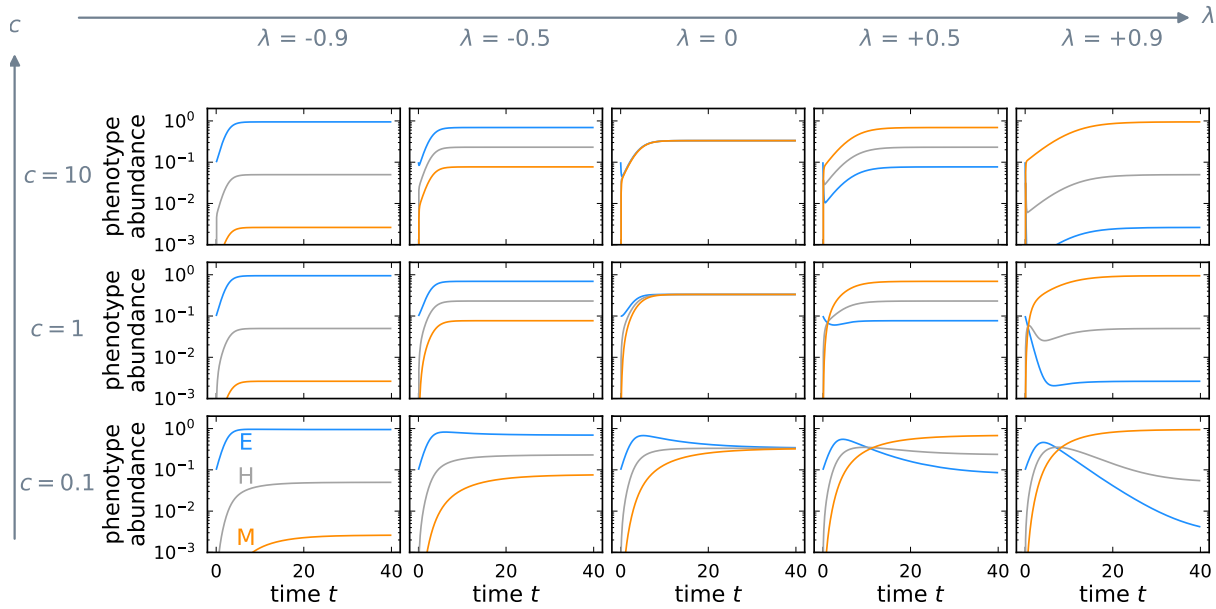

Figure 3: **The dynamics of equilibration are determined by the transition speed**. The panels show the simulated equilibration dynamics of tumor phenotypes from the same initial condition, $(x_1, x_2, x_3) = (\frac{1}{10}, 0, 0)$, for different combinations of transition speed c and transition bias λ. The transition speed c sets the pace of the transition dynamics relative to the growth dynamics. For any transition bias λ, the time to reach the stable phenotype distribution decreases as the transition speed increases.

The initial conditions determine the direction of phenotype shift

The stability of the coexistence equilibrium has interesting consequences for metastasis formation and epithelial-mesenchymal transitions. The primary site of the tumor at an early stage is composed mainly of proliferative epithelial cells. Thus, at the primary site, the stable phenotype distribution is approached by a relative increase in the abundance of mesenchymal-like cells, resulting in a change in the average phenotype of the tumor population (Fig. 4, first column). The secondary tumor site is initially founded by mesenchymal-like cells due to the selection pressure for invasive properties during dissemination. Therefore, the stable equilibrium is approached by a relative increase of epithelial-like cells at the secondary site, shifting the average population

phenotype towards the epithelial phenotype (Fig. 4, second column) during metastasis formation.

After a perturbation from the coexistence equilibrium, e.g., by treatment, the stable phenotype distribution is restored, compensating the effect of the perturbation (Fig. 4, columns three to five). Hence, the phenotypically plastic tumor cell population can maintain heterogeneity and is robust against interventions. Our model thus exhibits site- and treatment-specific phenotype shifts that result only from the selection during dissemination or treatment and are independent of the microenvironments of primary and secondary sites.

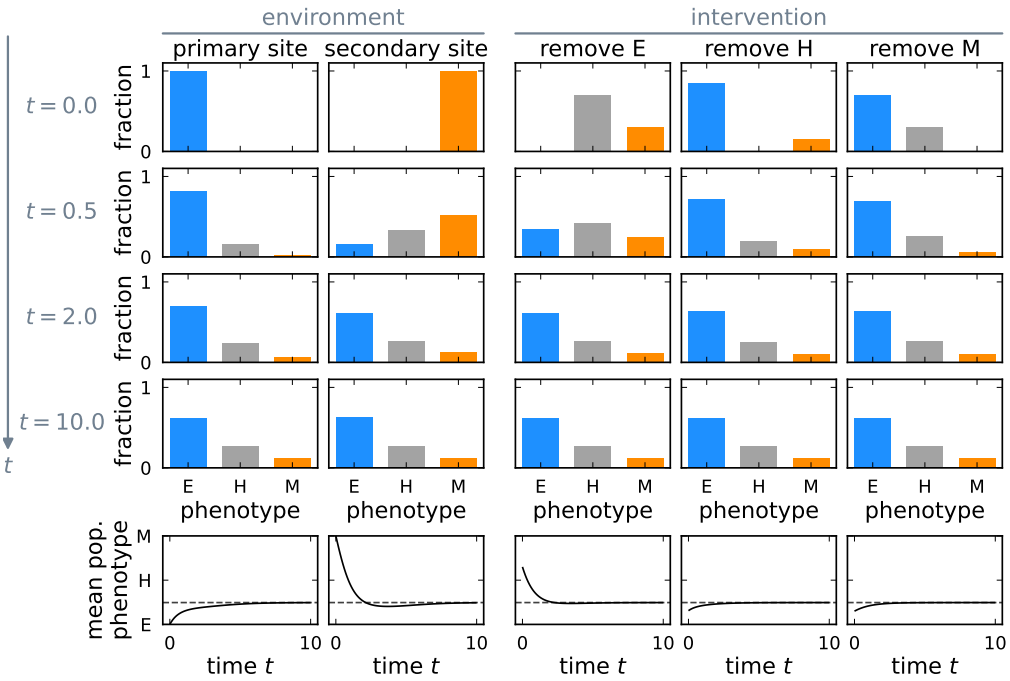

Figure 4: **Plasticity-driven equilibration of the phenotype distribution from different initial conditions**. Depending on the initial condition, the equilibration of the phenotype distribution proceeds along different paths (top four rows, the vertical axis represents time). The mean population phenotype over time is shown in the last row with its asymptote (dashed line). The first column shows the phenotype dynamics of a plastic tumor at the primary site, where it forms from initially only epithelial cells. The second column represents the growth of a metastasis after mainly mesenchymal cells have arrived at the secondary site. The last three columns show the dynamics after a hypothetical intervention that removes all epithelial, all hybrid, or all mesenchymal cells. In all cases, the tumor approaches the stable phenotype distribution; however, different initial conditions lead to shifting the average phenotype in different directions.

The type of treatment affects the phenotype distribution of the tumor

Next, we tested how the mean of the phenotype distribution changes during and after growth-dependent and growth-independent treatment (Fig. 5). Growth-dependent treatment targets proliferating cells, thus epithelial cells experience higher treatment-induced mortality (Fig. 5a), and the mean of the distribution shifts towards the mesenchymal phenotype (Fig. 5c). Growth-independent treatment targets all phenotypes equally, not changing the phenotype distribution

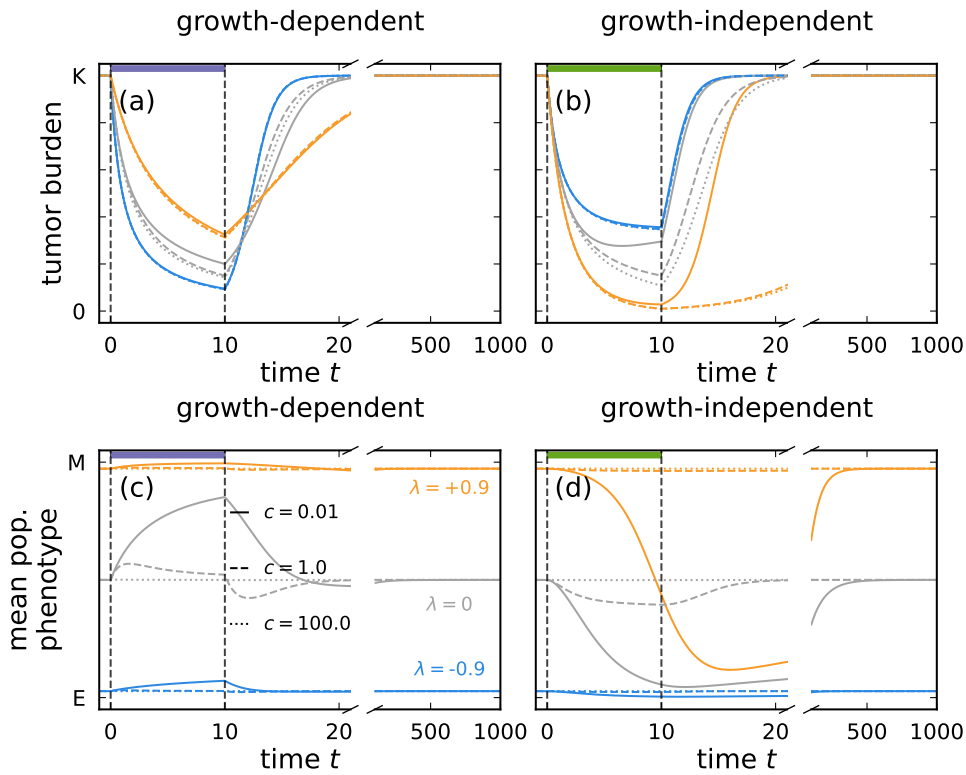

Figure 5: **Growth-dependent and growth-independent treatment can transiently alter the phenotype distribution of a tumor**. During treatment, the tumor burden reduces (panels a and b), and the mean phenotype of the tumor changes if the transition speed c is small but restores to the untreated mean phenotype after treatment (panels c and d). Treatment is applied between $t = 0$ and $t = 10$. Afterward, regrowth and equilibration of the phenotype distribution are tracked until $t = 1000$. The violet and green horizontal bars indicate growth-dependent and growth-independent treatments. Growth-dependent treatment shifts the mean of the phenotype distribution towards the mesenchymal phenotype as it exerts higher mortality on epithelial cells. Conversely, growth-independent treatment shifts the mean towards the epithelial phenotype as epithelial cells compensate for the mortality by faster growth.

directly. However, since the tumor is not at carrying capacity during treatment, this room for growth is filled by epithelial-like cells as they grow fast (Fig. 5b). Thus, during growth-independent treatment, the phenotype average shifts towards the epithelial phenotype, especially if transitions are slow compared to growth dynamics ($c < 1$, Fig. 5d). After treatment, the phenotype composition returns to the stable distribution that is purely determined by the transition bias (Eq. (2)). The restoration of the stable phenotype distribution is driven by regrowth of the suppressed phenotypes and therefore occurs considerably slower after growth-independent treatment, i.e., in the direction of a frequency increase of mesenchymal cells (Fig. 5d).

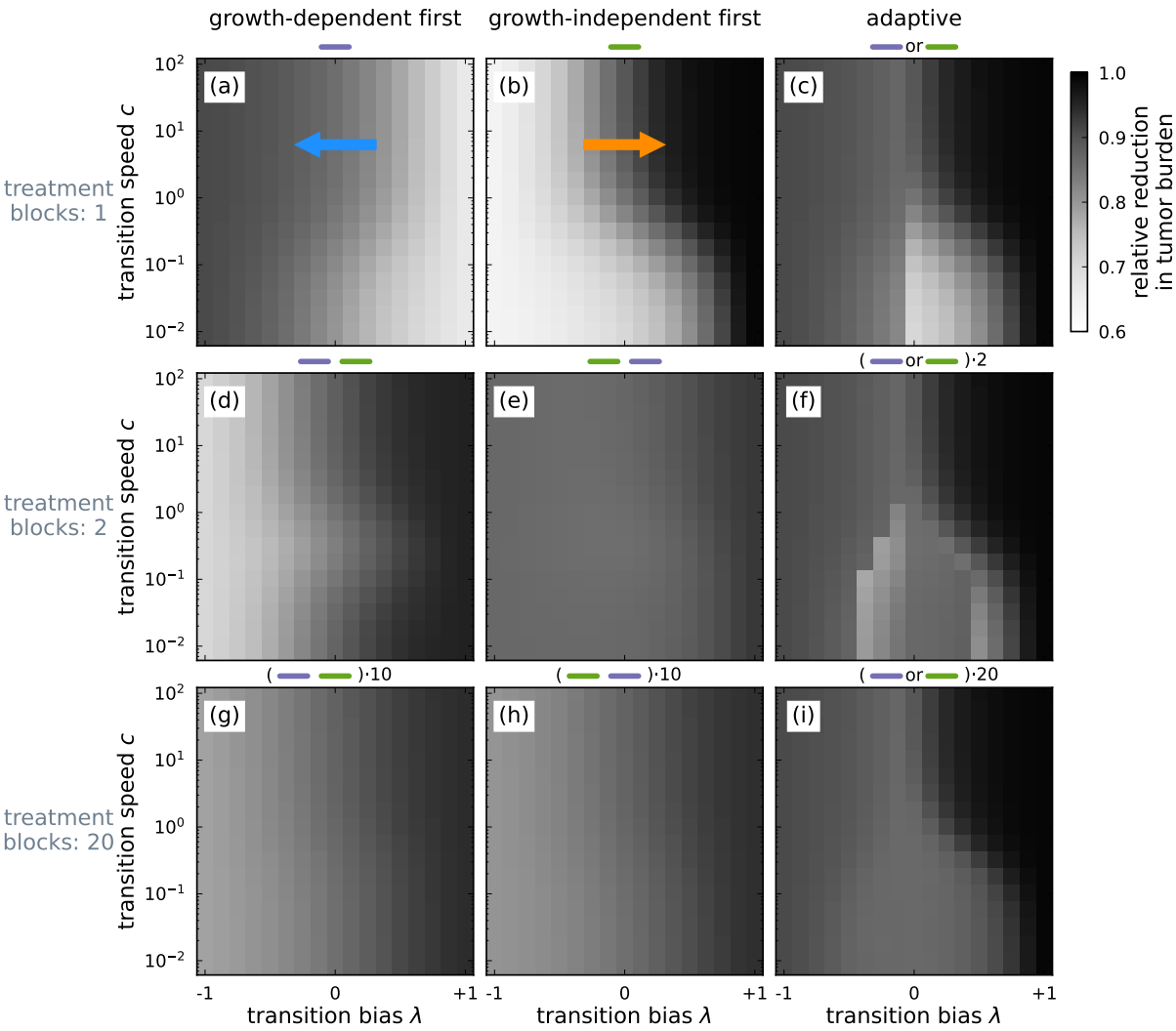

Figure 6: **Reduction in tumor burden for different sequential treatment schemes**. The reduction in tumor burden relative to the carrying capacity $\frac{\sum_{i=1}^{3} x_i - K}{K}$ for different combinations of transition bias λ and transition speed c is indicated by the brightness gradient. Darker colors represent a higher reduction and, thus, a better outcome. We evaluate the effect of splitting the treatment period into multiple treatment blocks (rows) and investigate different treatment schemes with either predefined or adaptive treatment sequences (columns). Adjuvant therapy can alter the phenotype transitions, which in our model translates to changes, for example, to the transition bias λ, indicated by the arrows in panels a and b.

The effect of single-block or sequential multi-block treatment schemes depends on phenotype composition and phenotype dynamics

Exploring a broader parameter space, we support the previous findings that the effect of growth-dependent and growth-independent treatment indeed depends strongly on transition bias and speed (Fig. 6). To explore the potential of leveraging the treatment-induced phenotype changes, we also investigated sequential treatment patterns that consist of multiple treatment blocks.

We find that one-block treatment schemes that match the phenotype distribution (i.e.

growth-dependent treatment for mainly epithelial phenotypes, $\lambda \to -1$, and growth-independent treatment for mainly mesenchymal phenotypes, $\lambda \to 1$) achieve the strongest reduction in tumor burden (Fig. 6, panels a and b). These phenotype-matched treatment combinations exert the highest mortality on the tumor population. Applying them for the whole treatment duration thus results in the highest reduction of tumor burden. Higher transition speeds c cause a faster replenishment of treatment-sensitive phenotypes from less sensitive phenotypes, entailing a cost of phenotypic plasticity. Thus, treatment efficacy improves for higher transition speeds for single-block treatments.

In the multi-block schemes (see Fig. S2 for tumor burden and mean phenotype dynamics of the two-block scheme), the application duration of the optimal treatment is reduced and thus results in a smaller reduction of these tumors at the extremes of the transition bias axis (Fig. 6, panels d and e). Frequent treatment alterations result in an intermediate tumor burden reduction across trait space which may be desirable if the characteristics of the tumor's phenotype distribution and thus transition bias λ and transition speed c are unknown (Fig. 6, panels g and h).

If, however, the phenotype distribution is known, the adaptive treatment scheme can be applied. This treatment scheme selects the treatment type that exerts the higher mortality on the tumor, given the phenotype distribution at the timepoint of treatment choice. We assume that initially, the phenotype distribution has reached its equilibrium given by Eq. (2), which is determined mainly by the transition bias λ. For the one-block adaptive treatment scheme only at the beginning of the treatment phase a treatment type has to be determined. Thus, the treatment type decision in the adaptive one-block treatment scheme depends only on the transition bias λ. For our parameters and assumptions on the growth rates of the phenotypes, the switch between applying the growth-dependent and the growth-independent treatment type occurs at $\tilde{\lambda} \approx -0.15$. Consequently, in the one-block adaptive treatment (Fig. 6c), the reductions of tumors with more epithelial cells, $\lambda < \tilde{\lambda}$, are identical to reductions obtained for the growth-dependent treatment type. Tumors with more mesenchymal cells, $\lambda > \tilde{\lambda}$, are affected by one-block adaptive treatment identically to the growth-independent treatment.

For the two-block adaptive treatment, the tumor reduction pattern is more intricate (Fig. 6f). At $\lambda > \tilde{\lambda}$, the mortality exerted by growth-independent treatment is higher; thus, growth-independent treatment is chosen as the first treatment type. At large transition speed c and high transition bias λ, growth-independent treatment is also chosen for the second treatment block. Only for a transition bias slightly exceeding $\tilde{\lambda}$ and small c, a treatment switch occurs, and the tumor burden reduction is higher than in the single-block scheme. For $\lambda < \tilde{\lambda}$, the first treatment type is growth-dependent treatment. Only for small c and close to $\tilde{\lambda}$ the treatment type is switched after half the treatment period, which interestingly worsens the tumor burden reduction compared to a single block of only growth-dependent treatment. This choice is possible as the decision criterion for treatment choice is the instantaneous mortality and does not account for the potential future tumor size or the future phenotype distribution, or mortality integrated over time. Since the growth-independent treatment exerts no selection pressure against the proliferative phenotype, switching to this treatment type comes at the risk that soon after the switch, the phenotype distribution will have shifted to a larger epithelial proportion, where the growth-independent treatment is less effective than the growth-dependent treatment. Increasing

the number of treatment blocks mediates this risk and achieves the highest tumor burden reduction for small c and intermediate λ in the adaptive treatment scheme.

Different modeling assumptions (unequal competitiveness of phenotypes or phenotype-dependent transition speed) change the effect of treatment only quantitatively (supplementary text, Sections 5.3.1 and 5.3.2, Figs. S5 and S8).

The potential of adjuvant treatment

Modifying the process of phenotype transition with adjuvant therapies promises to alter the phenotype distribution of a tumor. In our model, a more epithelial phenotype distribution is achieved by an adjuvant drug that decreases the transition bias towards mesenchymal phenotypes λ. Contrarily, a more mesenchymal phenotype distribution is achieved by increasing the transition bias. Fig. 6 indicates how modifying the transition bias λ with adjuvant drugs can affect the predicted reduction in tumor burden. We find that the tumor burden is more strongly reduced if a single block of growth-dependent treatment is accompanied by an adjuvant drug that makes the tumor more epithelial by decreasing the transition bias λ (arrow in Fig. 6a). Contrastingly, the effect of the growth-independent treatment can be enhanced by an adjuvant drug that makes the tumor more mesenchymal by increasing the transition bias λ (arrow in Fig. 6b). For multi-block treatment schemes, we find that increasing λ generally also increases the reduction in tumor burden, albeit this effect depends on the point in parameter space for the adaptive treatment. Adjuvant therapies that increase the transition speed c increase the treatment effect for a single treatment block, but for two treatment blocks predictions are more difficult as they depend on the treatment sequence and the system parameters.

4 Discussion

Cancer cell plasticity increases tumor heterogeneity, facilitates metastasis formation, and often hinders treatment approaches (Deshmukh and Saini, 2020). We formulated a mathematical model of plastic phenotype transitions that result in a stable and heterogeneous phenotype distribution, mainly determined by the bias of phenotype transitions. The stability of this phenotype distribution implies that perturbations to this distribution will be reverted, which has interesting consequences for our understanding of phenotype changes during metastasis formation and treatment.

During metastasis formation, one prominent phenotype transition of cancer cells is the epithelial-mesenchymal transition (Nieto et al., 2016; Jolly et al., 2017). At the primary site of cancer origin, the initial cancer cell population consists mainly of proliferative epithelial cells and thus approaches the stable phenotype distribution prescribed by plasticity by a relative increase of cells with a more mesenchymal phenotype, according to our model. During metastasis formation, selection for motility and invasiveness during the dissemination of cancer cells increases the frequency of the mesenchymal phenotype in the cancer cell population. Therefore, the arriving population at the secondary site is mainly constituted of mesenchymal phenotype and approaches the stable phenotype distribution by a relative increase of cells with a more epithelial phenotype. Thus, we find that the same process, phenotypic plasticity, can

be responsible for both the epithelial-mesenchymal transition at the primary site as well as the mesenchymal-epithelial transition at the secondary site, even without necessarily different microenvironments at the primary and secondary site. However, microenvironmental differences undoubtedly exacerbate phenotypic changes during the dissemination from primary to secondary site (Group Young Researchers in Inflammatory Carcinogenesis et al., 2021). Indeed, we can capture much more pronounced phenotype changes by assuming different transition biases λ at primary and secondary sites, resulting in differing stable phenotype distributions.

Our model suggests that the stable equilibrium is also responsible for generating and maintaining intra-tumor heterogeneity during and after treatment. There have been recent theoretical studies to treat phenotypically heterogeneous tumors (Viossat and Noble, 2021; Raatz et al., 2021; Cassidy et al., 2021) with some experiments to support them (Li and Thirumalai, 2022). These strategies aim to remove or reduce the tumor burden and delay tumor relapse. However, these studies do not target or capitalize on the source of the heterogeneity. We investigated growth-dependent and growth-independent treatment types, capturing some of the mechanisms of chemo- and immunotherapy. We found that the transition bias, and thus the shape of the stable phenotype distribution, determines which treatment type or sequence of different treatment types is most effective. Our model predicts a higher efficiency of growth-dependent treatment for a transition bias towards epithelial phenotypes. Growth-independent treatment becomes more effective for more a transition bias towards mesenchymal phenotypes. This connection between treatment success and the shape of the phenotype distribution can be understood better by considering the distribution's mean, variance, and skewness. Narrow phenotype distributions are well characterized by their mean, which can be used to match treatment type and phenotype. For example, chemotherapy will be the most effective when there are only proliferative cells. Such a phenotype-matched treatment will perform well for homogeneous tumors without mismatching terminal phenotypes. However, tumors are often heterogeneous, weakening their treatment response (Greenbaum et al., 2019; McDonald et al., 2019). Describing such a tumor with multiple distinct phenotypes necessitates accounting also for the variance of the phenotype distribution as a proxy for tumor heterogeneity. Also in our results, the presence of terminal phenotypes that are not phenotype-matched with the main treatment weakens the reduction in tumor burden. Interestingly, the skewness of the phenotype distribution captures this mismatch between the treatment type and the abundance of terminal phenotypes that are not matched by the treatment, as they are far off the mean of the phenotype distribution. When matching the treatment to the mean of the phenotype distribution, an increasing skewness thus signals the onset of relapse from mismatched phenotypes. In our model, the variance of the stable phenotype distribution, i.e., the phenotypic heterogeneity, is maximal when there is no transition bias, i.e., $\lambda = 0$. The skewness, i.e., the mismatch between targeted phenotype and unmatched terminal phenotypes, is largest at extreme transition biases ($\lambda \to -1$ or $\lambda \to 1$). Accordingly, our model predicts a sweet spot for controlling both heterogeneity and mismatched terminal phenotypes at an intermediate transition bias, $0 < |\lambda| < 1$.

The relation between treatment success and phenotype dynamics can potentially be exploited during cancer treatment as the transition bias and, therefore, the stable phenotype distribution can be modulated by adjuvant therapy. In the context of epithelial-mesenchymal plasticity,

the molecular drivers of the epithelial-mesenchymal transition and the mesenchymal-epithelial transitions are known (Dongre and Weinberg, 2019; Subbalakshmi et al., 2021). Translating to our model, the concentration of these molecular drivers controls the transition bias λ and transition speed c. Altering the concentrations of these drivers in the tumor microenvironment would thus translate to changing these parameters that are decisive for the phenotype transition process. Therefore, it may be possible to regulate tumor phenotypes, reduce metastasis, and achieve a better treatment response by controlling the transition bias with an adjuvant treatment which, for example has been shown with TGF-β blockage (Liu et al., 2012; Pickup et al., 2013; Lee et al., 2022).

Building on the decisive effect of such molecules for the phenotype transitions and heterogeneity, their concentration could also be used to characterize tumor heterogeneity. Measuring their concentrations might be practically more feasible than measuring phenotype abundances. For example, in the case of TGF-β driven epithelial-mesenchymal transition, the tumor could be characterized by the concentration of TGF-β instead of quantifying the number of epithelial, hybrid, and mesenchymal cells. The concentration of the molecular driver could then be used for the prediction of prognosis. Additionally, if available, the skewness of the phenotype distribution, i.e., the abundance of mismatched phenotypes, can characterize the relapse. For example, the relapse of a primarily epithelial tumor that has positive skewness and is treated with growth-dependent treatment will initially be driven by the growth of mesenchymal cells before, eventually, the epithelial cells take over the cancer cell population, leading to a biphasic relapse dynamics (Raatz et al., 2021).

In this study, we formulated a mathematical model that describes phenotypically plastic cancer cell populations. We found that the heterogeneity generated by this inherent plasticity can explain the transitions between epithelial and mesenchymal phenotypes, which are known to facilitate cancer progression and metastasis (Gupta and Massagué, 2006; Zheng et al., 2015; Turajlic and Swanton, 2016; Jolly et al., 2017; Fares et al., 2020; Esposito et al., 2021). Our model provides an alternative hypothesis to the factors driving such transitions which does not rely on microenvironmental differences, but on selection pressures during dissemination followed by the restoration of the stable phenotype distribution. Finally, our study suggests modulating the phenotype transitions with adjuvant treatment and then applying phenotype-matched treatment types to not only mitigate but also leverage plasticity as an inherent component of cancer cell populations.

Acknowledgements

All authors acknowledge funding by Deutsche Forschungsgemeinschaft through the Research Training Group "Translational Evolutionary Research" (TransEvo) (Project number 400993799, `https://gepris.dfg.de/gepris/projekt/400993799`) and funding by the Deutsche Krebshilfe (AZ 70112935) to Susanne Sebens. Sa.Sh. is grateful to Dr. Stefano Giaimo and Saptarshi Pal for the discussions on stability.

Author contributions

Role	Contributor
Conceptualization	Sa.Sh., M.R., A.T., Su.Se., L.M.P.
Methodology	Sa.Sh., M.R., A.T.
Software	Sa.Sh.
Investigation	Sa.Sh., M.R., A.T.
Visualization	Sa.Sh.
Writing-original draft	Sa.Sh., M.R.
Writing-review and editing	Sa.Sh., M.R., A.T., Su.Se., L.M.P.
Supervision and project administration	M.R., A.T.

Competing interests

The authors declare no competing interests.

References

David Basanta and Alexander R. A. Anderson. Exploiting ecological principles to better understand cancer progression and treatment. *Interface Focus*, 3(4):20130020–20130020, 2013. doi: 10.1098/rsfs.2013.0020.

Francisco Caiado, Bruno Silva-Santos, and Håkan Norell. Intra-tumour heterogeneity – going beyond genetics. *FEBS Journal*, 283(12):2245–2258, 2016.

Tyler Cassidy, Daniel Nichol, Mark Robertson-Tessi, Morgan Craig, and Alexander R. A. Anderson. The role of memory in non-genetic inheritance and its impact on cancer treatment resistance. *PLOS Computational Biology*, 17(8):e1009348, August 2021. ISSN 1553-7358. doi: 10.1371/journal.pcbi.1009348.

Saniya Deshmukh and Supreet Saini. Phenotypic Heterogeneity in Tumor Progression, and Its Possible Role in the Onset of Cancer. *Frontiers in Genetics*, 11:604528, November 2020. ISSN 1664-8021. doi: 10.3389/fgene.2020.604528.

Hanna Dillekås, Michael S. Rogers, and Oddbjørn Straume. Are 90% of deaths from cancer caused by metastases? *Cancer Medicine*, 8(12):5574–5576, September 2019. ISSN 2045-7634, 2045-7634. doi: 10.1002/cam4.2474.

Anushka Dongre and Robert A. Weinberg. New insights into the mechanisms of epithelial–mesenchymal transition and implications for cancer. *Nature Reviews Molecular Cell Biology*, 20(2):69–84, February 2019. ISSN 1471-0072, 1471-0080. doi: 10.1038/s41580-018-0080-4.

Mark Esposito, Shridar Ganesan, and Yibin Kang. Emerging strategies for treating metastasis. *Nature Cancer*, 2(3): 258–270, March 2021. ISSN 2662-1347. doi: 10.1038/s43018-021-00181-0.

Jawad Fares, Mohamad Y. Fares, Hussein H. Khachfe, Hamza A. Salhab, and Youssef Fares. Molecular principles of metastasis: A hallmark of cancer revisited. *Signal Transduction and Targeted Therapy*, 5(1):28, December 2020. ISSN 2059-3635. doi: 10.1038/s41392-020-0134-x.

Beat B. Fischer, Marek Kwiatkowski, Martin Ackermann, Jasmin Krismer, Severin Roffler, Marc J. F. Suter, Rik I. L. Eggen, and Blake Matthews. Phenotypic plasticity influences the eco-evolutionary dynamics of a predator–prey system. *Ecology*, 95(11):3080–3092, November 2014. ISSN 0012-9658. doi: 10.1890/14-0116.1.

Linnea C Franssen and Mark A J Chaplain. A mathematical multi-organ model for bidirectional epithelial–mesenchymal transitions in the metastatic spread of cancer. *IMA Journal of Applied Mathematics*, 85(5):724–761, September 2020. ISSN 0272-4960, 1464-3634. doi: 10.1093/imamat/hxaa022.

Feliks R. Gantmacher. *The Theory of Matrices. Vol. 2*, volume 2. American Mathematical Soc, Providence, RI, reprinted edition, 2009. ISBN 978-0-8218-2664-5.

Alf Giese, Melinda A. Loo, Nhan Tran, Dorothy Haskett, Stephen W. Coons, and Michael E. Berens. Dichotomy of astrocytoma migration and proliferation. *International Journal of Cancer*, 67(2):275–282, July 1996. ISSN 00207136, 10970215. doi: 10.1002/(sici)1097-0215(19960717)67:2<275::aid-ijc20>3.0.co;2-9.

Alissa Greenbaum, David R. Martin, Thèrése Bocklage, Ji-Hyun Lee, Scott A. Ness, and Ashwani Rajput. Tumor Heterogeneity as a Predictor of Response to Neoadjuvant Chemotherapy in Locally Advanced Rectal Cancer. *Clinical Colorectal Cancer*, 18(2):102–109, June 2019. ISSN 15330028. doi: 10.1016/j.clcc.2019.02.003.

Group Young Researchers in Inflammatory Carcinogenesis, Anna Maxi Wandmacher, Anne-Sophie Mehdorn, and Susanne Sebens. The Heterogeneity of the Tumor Microenvironment as Essential Determinant of Development, Progression and Therapy Response of Pancreatic Cancer. *Cancers*, 13(19):4932, September 2021. ISSN 2072-6694. doi: 10.3390/cancers13194932.

Gaorav P. Gupta and Joan Massagué. Cancer Metastasis: Building a Framework. *Cell*, 127(4):679–695, November 2006. ISSN 00928674. doi: 10.1016/j.cell.2006.11.001.

Piyush B. Gupta, Christine M. Fillmore, Guozhi Jiang, Sagi D. Shapira, Kai Tao, Charlotte Kuperwasser, and Eric S. Lander. Stochastic State Transitions Give Rise to Phenotypic Equilibrium in Populations of Cancer Cells. *Cell*, 146(4): 633–644, August 2011. ISSN 00928674. doi: 10.1016/j.cell.2011.07.026.

Charles R. Harris, K. Jarrod Millman, Stéfan J. van der Walt, Ralf Gommers, Pauli Virtanen, David Cournapeau, Eric Wieser, Julian Taylor, Sebastian Berg, Nathaniel J. Smith, Robert Kern, Matti Picus, Stephan Hoyer, Marten H. van Kerkwijk, Matthew Brett, Allan Haldane, Jaime Fernández del Río, Mark Wiebe, Pearu Peterson, Pierre Gérard-Marchant, Kevin Sheppard, Tyler Reddy, Warren Weckesser, Hameer Abbasi, Christoph Gohlke, and Travis E. Oliphant. Array programming with NumPy. *Nature*, 585(7825):357–362, September 2020. ISSN 0028-0836, 1476-4687. doi: 10.1038/s41586-020-2649-2.

Josef Hofbauer and Karl Sigmund. *Evolutionary Games and Population Dynamics*. Cambridge University Press, Cambridge, UK, first edition, May 1998. ISBN 978-0-521-62365-0 978-0-521-62570-8 978-1-139-17317-9. doi: 10.1017/cbo9781139173179.

Deli Hong, Andrew J. Fritz, Sayyed K. Zaidi, Andre J. Wijnen, Jeffrey A. Nickerson, Anthony N. Imbalzano, Jane B. Lian, Janet L. Stein, and Gary S. Stein. Epithelial-to-mesenchymal transition and cancer stem cells contribute to breast cancer heterogeneity. *Journal of Cellular Physiology*, 233(12):9136–9144, December 2018. ISSN 0021-9541, 1097-4652. doi: 10.1002/jcp.26847.

John D. Hunter. Matplotlib: A 2D Graphics Environment. *Computing in Science & Engineering*, 9(3):90–95, 2007. ISSN 1521-9615. doi: 10.1109/mcse.2007.55.

Mohit Kumar Jolly, Kathryn E. Ware, Shivee Gilja, Jason A. Somarelli, and Herbert Levine. EMT and MET: Necessary or permissive for metastasis? *Molecular Oncology*, 11(7):755–769, July 2017. ISSN 1574-7891, 1878-0261. doi: 10.1002/1878-0261.12083.

Mohit Kumar Jolly, Sendurai A. Mani, and Herbert Levine. Hybrid epithelial/mesenchymal phenotype(s): The 'fittest' for metastasis? *Biochimica et Biophysica Acta (BBA) - Reviews on Cancer*, 1870(2):151–157, December 2018. ISSN 0304419x. doi: 10.1016/j.bbcan.2018.07.001.

Kirill S. Korolev, Joao B. Xavier, and Jeff Gore. Turning ecology and evolution against cancer. *Nat Rev Cancer*, 14(5): 371–380, 2014.

Hyang-Mi Lee, Hye-Jin Lee, and Ji-Eun Chang. Inflammatory Cytokine: An Attractive Target for Cancer Treatment. *Biomedicines*, 10(9):2116, August 2022. ISSN 2227-9059. doi: 10.3390/biomedicines10092116.

Xin Li and D. Thirumalai. A mathematical model for phenotypic heterogeneity in breast cancer with implications for therapeutic strategies. *Journal of The Royal Society Interface*, 19(186):20210803, January 2022. ISSN 1742-5662. doi: 10.1098/rsif.2021.0803.

Jieqiong Liu, Shan Liao, Benjamin Diop-Frimpong, Wei Chen, Shom Goel, Kamila Naxerova, Marek Ancukiewicz, Yves Boucher, Rakesh K. Jain, and Lei Xu. TGF-β blockade improves the distribution and efficacy of therapeutics in breast carcinoma by normalizing the tumor stroma. *Proceedings of the National Academy of Sciences*, 109(41):16618–16623, October 2012. ISSN 0027-8424, 1091-6490. doi: 10.1073/pnas.1117610109.

Bo Ma, Alan Wells, and Amanda M. Clark. The pan-therapeutic resistance of disseminated tumor cells: Role of phenotypic plasticity and the metastatic microenvironment. *Seminars in Cancer Biology*, 60:138–147, February 2020. ISSN 1044579x. doi: 10.1016/j.semcancer.2019.07.021.

Kerry-Ann McDonald, Tsutomu Kawaguchi, Qianya Qi, Xuan Peng, Mariko Asaoka, Jessica Young, Mateusz Opyrchal, Li Yan, Santosh Patnaik, Eigo Otsuji, and Kazuaki Takabe. Tumor Heterogeneity Correlates with Less Immune Response and Worse Survival in Breast Cancer Patients. *Annals of Surgical Oncology*, 26(7):2191–2199, July 2019. ISSN 1068-9265, 1534-4681. doi: 10.1245/s10434-019-07338-3.

M. Angela Nieto, Ruby Yun-Ju Huang, Rebecca A. Jackson, and Jean Paul Thiery. Emt: 2016. *Cell*, 166(1):21–45, June 2016. ISSN 00928674. doi: 10.1016/j.cell.2016.06.028.

E.R. Pianka. On r- and k-selection. *The American Naturalist*, 104(940):592–597, 1970.

Michael Pickup, Sergey Novitskiy, and Harold L. Moses. The roles of TGFβ in the tumour microenvironment. *Nature Reviews Cancer*, 13(11):788–799, November 2013. ISSN 1474-175X, 1474-1768. doi: 10.1038/nrc3603.

M. Raatz, S. Shah, G. Chitadze, M. Brüggemann, and A. Traulsen. The impact of phenotypic heterogeneity of tumour cells on treatment and relapse dynamics. *PLoS Computational Biology*, 17(2):e1008702, 2021.

Yelyzaveta Shlyakhtina, Katherine L. Moran, and Maximiliano M. Portal. Genetic and Non-Genetic Mechanisms Underlying Cancer Evolution. *Cancers*, 13(6):1380, March 2021. ISSN 2072-6694. doi: 10.3390/cancers13061380.

Rebecca L. Siegel, Kimberly D. Miller, and Ahmedin Jemal. Cancer statistics, 2020. *CA: A Cancer Journal for Clinicians*, 70(1):7–30, January 2020. ISSN 0007-9235, 1542-4863. doi: 10.3322/caac.21590.

S. Smale. On the differential equations of species in competition. *Journal of Mathematical Biology*, 3(1):5–7, 1976. ISSN 0303-6812, 1432-1416. doi: 10.1007/bf00307854.

Steven H. Strogatz. *Nonlinear Dynamics and Chaos*. CRC Press, zeroth edition, May 2018. ISBN 978-0-429-96111-3. doi: 10.1201/9780429492563.

Ayalur Raghu Subbalakshmi, Sarthak Sahoo, Isabelle McMullen, Aaditya Narayan Saxena, Sudhanva Kalasapura Venugopal, Jason A. Somarelli, and Mohit Kumar Jolly. KLF4 Induces Mesenchymal–Epithelial Transition (MET) by Suppressing Multiple EMT-Inducing Transcription Factors. *Cancers*, 13(20):5135, October 2021. ISSN 2072-6694. doi: 10.3390/cancers13205135.

Hyuna Sung, Jacques Ferlay, Rebecca L. Siegel, Mathieu Laversanne, Isabelle Soerjomataram, Ahmedin Jemal, and Freddie Bray. Global Cancer Statistics 2020: GLOBOCAN Estimates of Incidence and Mortality Worldwide for 36 Cancers in 185 Countries. *CA: A Cancer Journal for Clinicians*, 71(3):209–249, May 2021. ISSN 0007-9235, 1542-4863. doi: 10.3322/caac.21660.

S. Turajlic and C. Swanton. Metastasis as an evolutionary process. *Science*, 352(6282):169–175, April 2016. ISSN 0036-8075, 1095-9203. doi: 10.1126/science.aaf2784.

Guido van Rossum and Fred L. Drake. *The Python Language Reference*. Number Pt. 2 in Python Documentation Manual / Guido van Rossum; Fred L. Drake [Ed.]. Python Software Foundation, Hampton, NH, release 3.0.1 [repr.] edition, 2010. ISBN 978-1-4414-1269-0.

Yannick Viossat and Robert Noble. A theoretical analysis of tumour containment. *Nature Ecology & Evolution*, April 2021. doi: 10.1038/s41559-021-01428-w.

Pauli Virtanen, Ralf Gommers, Travis E. Oliphant, Matt Haberland, Tyler Reddy, David Cournapeau, Evgeni Burovski, Pearu Peterson, Warren Weckesser, Jonathan Bright, Stéfan J. van der Walt, Matthew Brett, Joshua Wilson, K. Jarrod Millman, Nikolay Mayorov, Andrew R.J. Nelson, Eric Jones, Robert Kern, Eric Larson, C. J. Carey, İlhan Polat, Yu Feng, Eric W. Moore, Jake VanderPlas, Denis Laxalde, Josef Perktold, Robert Cimrman, Ian Henriksen, E. A. Quintero, Charles R. Harris, Anne M. Archibald, Antônio H. Ribeiro, Fabian Pedregosa, Paul van Mulbregt, Aditya Vijaykumar, Alessandro Pietro Bardelli, Alex Rothberg, Andreas Hilboll, Andreas Kloeckner, Anthony Scopatz, Antony Lee, Ariel Rokem, C. Nathan Woods, Chad Fulton, Charles Masson, Christian Häggström, Clark Fitzgerald, David A. Nicholson, David R. Hagen, Dmitrii V. Pasechnik, Emanuele Olivetti, Eric Martin, Eric Wieser, Fabrice Silva, Felix Lenders, Florian Wilhelm, G. Young, Gavin A. Price, Gert Ludwig Ingold, Gregory E. Allen, Gregory R. Lee, Hervé Audren, Irvin Probst, Jörg P. Dietrich, Jacob Silterra, James T. Webber, Janko Slavič, Joel Nothman, Johannes Buchner, Johannes Kulick, Johannes L. Schönberger, José Vinícius de Miranda Cardoso, Joscha Reimer, Joseph Harrington, Juan Luis Cano Rodríguez, Juan Nunez-Iglesias, Justin Kuczynski, Kevin Tritz, Martin Thoma, Matthew Newville,

Matthias Kümmerer, Maximilian Bolingbroke, Michael Tartre, Mikhail Pak, Nathaniel J. Smith, Nikolai Nowaczyk, Nikolay Shebanov, Oleksandr Pavlyk, Per A. Brodtkorb, Perry Lee, Robert T. McGibbon, Roman Feldbauer, Sam Lewis, Sam Tygier, Scott Sievert, Sebastiano Vigna, Stefan Peterson, Surhud More, Tadeusz Pudlik, Takuya Oshima, Thomas J. Pingel, Thomas P. Robitaille, Thomas Spura, Thouis R. Jones, Tim Cera, Tim Leslie, Tiziano Zito, Tom Krauss, Utkarsh Upadhyay, Yaroslav O. Halchenko, and Yoshiki Vázquez-Baeza. SciPy 1.0: fundamental algorithms for scientific computing in Python. *Nat Methods*, 17(3):261–272, 2020.

Robert A. Weinberg. *The Biology of Cancer*. Garland Science, Taylor & Francis Group, New York, second edition edition, 2014. ISBN 978-0-8153-4219-9 978-0-8153-4220-5.

M J West-Eberhard. Phenotypic Plasticity and the Origins of Diversity. *Annual Review of Ecology and Systematics*, 20(1): 249–278, November 1989. ISSN 0066-4162. doi: 10.1146/annurev.es.20.110189.001341.

Inc. Wolfram Research. Mathematica, Version 12.1, 2020. Champaign, IL, 2020.

Xiaofeng Zheng, Julienne L. Carstens, Jiha Kim, Matthew Scheible, Judith Kaye, Hikaru Sugimoto, Chia-Chin Wu, Valerie S. LeBleu, and Raghu Kalluri. Epithelial-to-mesenchymal transition is dispensable for metastasis but induces chemoresistance in pancreatic cancer. *Nature*, 527(7579):525–530, November 2015. ISSN 0028-0836, 1476-4687. doi: 10.1038/nature16064.

D. Zhou, Y. Luo, D. Dingli, and A. Traulsen. The invasion of de-differentiating cancer cells into hierarchical tissues. *PLoS Computational Biology*, 15:e1007167, 2019.

5 Supplementary

5.1 Supplementary figures

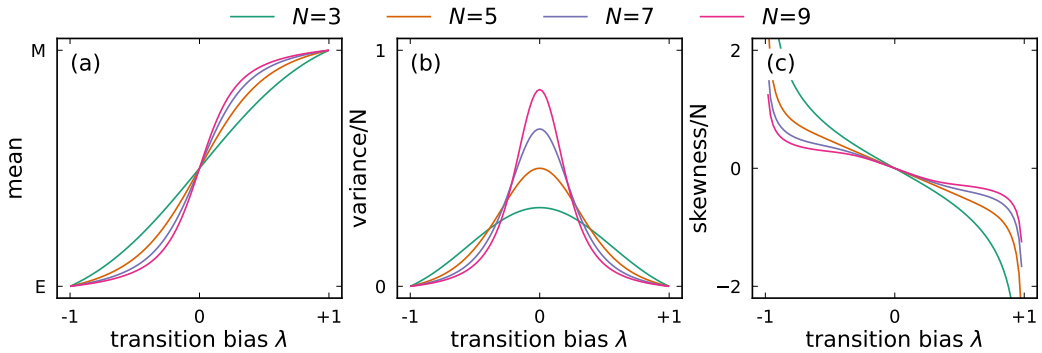

Figure S1: **The transition bias affects the phenotypic heterogeneity and abundances of terminal phenotypes**. The stable phenotype distribution $\Pr(i \mid \lambda, N) = \frac{x_i^*}{K}$, written as a function of transition bias λ for different numbers of phenotypes N, can be well characterized by its mean, variance and skewness. The mean allows the identification of phenotype-matched treatment, e.g., select growth-dependent treatment for mainly epithelial tumors. Variance represents a proxy for phenotypic heterogeneity, which often impedes treatment success. Skewness is a proxy for the abundance of terminal phenotypes far off the mean that are potentially unmatched by treatment. An intermediate transition bias, $0 < |\lambda| < 1$, minimizes both the heterogeneity and the presence of potentially unmatched terminal phenotypes, indicated by a combination of small variance and a small absolute value of skewness.

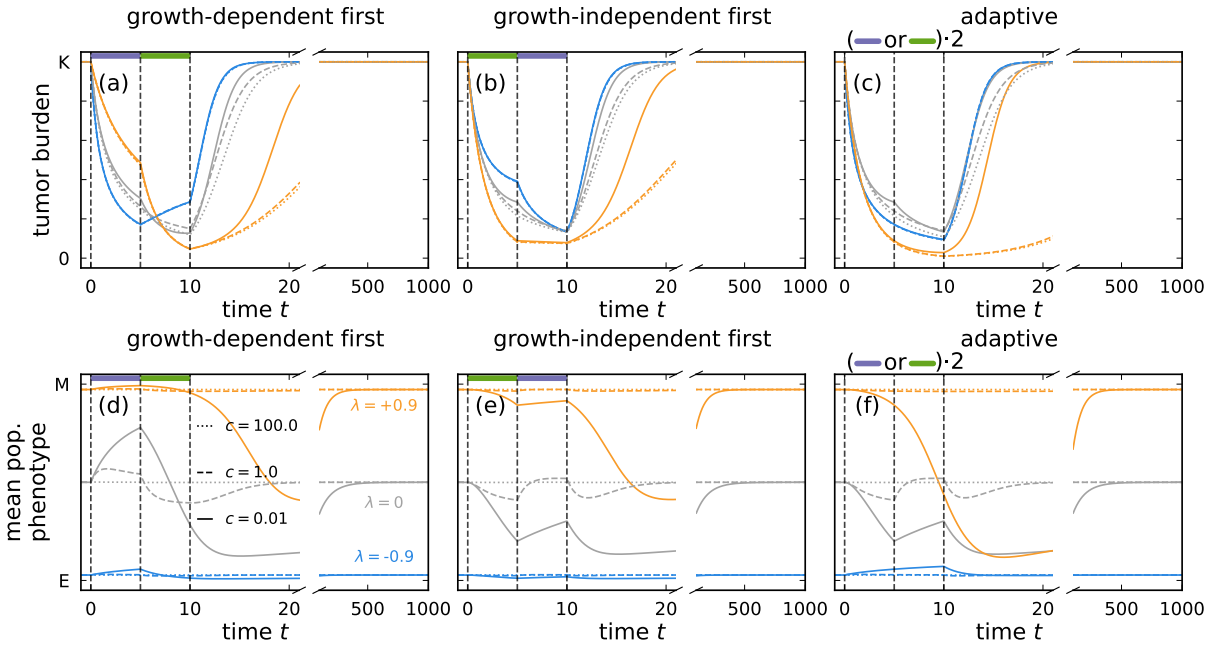

Figure S2: **Changing treatment types can increase the efficacy of treatment**. The figure shows the effect of sequential two-block treatment on the total tumor abundance (first row) and mean phenotype (second row) during and after treatment. The growth-dependent treatment block is depicted by a violet bar, and the growth-independent block is shown by a green bar. The first block is applied between $t = 0$ and $t = 5$, and the second block is applied between $t = 5$ and $t = 10$. Tumor regrowth and equilibration of the phenotype distribution are tracked until $t = 1000$. When applying the adaptive treatment scheme, growth-dependent treatment is chosen for both blocks if the transition bias is low ($\lambda = -0.9$, blue lines). For unbiased, slow transitions ($\lambda = 0$ and $c = 0.01$), the treatment type switches from growth-independent to growth-dependent between the first and the second block (solid grey line). The growth-independent treatment type is applied in both treatment blocks for all other parameter combinations. Compared to single-block treatments (Fig. 5), tumor burden reductions at the end of the treatment phase can be higher or lower in two-block treatment schemes, depending on the transition bias and transition speeds, mirroring the complex patterns in Fig. 6. Two-block treatments are thus not always beneficial but can also reduce treatment efficacy if the treatment is not matched with the phenotype distribution.

5.2 Stability of the coexistence equilibrium

We analytically investigate the stability of the coexistence phenotype distribution (Eq. (2)) by linear stability analysis for $N = 2$ and $N = 3$ (Strogatz, 2018). For $N > 3$, we compute the eigenvalues using the script (`linear_stability.nb`, Supplementary Material) and observe that they are negative for our parameter ranges.

5.2.1 Two phenotypes $N = 2$

The following differential equations describe the system with two phenotypes without treatment.

$$\begin{aligned} \frac{dx_1}{dt} &= r_1\ x_1 \left(1 - \frac{x_1 + x_2}{K}\right) - c\ r_1\ (1+\lambda)\ x_1 + c\ r_2\ (1-\lambda)\ x_2 \\ \frac{dx_2}{dt} &= r_2\ x_2 \left(1 - \frac{x_1 + x_2}{K}\right) + c\ r_1\ (1+\lambda)\ x_1 - c\ r_2\ (1-\lambda)\ x_2 \end{aligned} \tag{S1}$$

The Jacobian of the system at a point (x_1, x_2) is

$$J = \begin{bmatrix} r_1\ \left(1 - \frac{x_1+x_2}{K}\right) - r_1\ \frac{x_1}{K} - c\ (1+\lambda)\ r_1 & c\ (1-\lambda)\ r_1 - r_1\ \frac{x_1}{K} \\ c\ (1+\lambda)\ r_1 - r_2 \frac{x_2}{K} & r_2\ \left(1 - \frac{x_1+x_2}{K}\right) - c\ (1-\lambda)\ r_1 - r_2 \frac{x_2}{K} \end{bmatrix} \tag{S2}$$

Evaluating the Jacobian at the coexistence equilibrium, $(x_1^*, x_2^*) = \frac{1}{2}K(1-\lambda, 1+\lambda)$, and using $r_2 = r_1 - (r_1 - r_N) = \frac{1}{5}r_1$ we get

$$J^* = \begin{bmatrix} -r_1\ (2c\ (1+\lambda) + 1 - \lambda) & \frac{1}{2}r_1\ (2c-1)(1-\lambda) \\ \frac{1}{10}r_1\ (10\ c - 1)(1+\lambda) & -\frac{1}{10}r_1\ (10c\ (1-\lambda) + 1 + \lambda) \end{bmatrix} \tag{S3}$$

The eigenvalues of this matrix are $-c\ r_1$ and $-\frac{1}{5}(2\lambda - 3)r_1$. By definition, growth rate r_1 and transition speed c both are positive. Thus, growth rate r_1 and transition speed c cannot affect the stability of the system with two phenotypes, $N = 2$. Thus, for simplicity we put $r = 1$ and $c = 1$, and get

$$J^* = \begin{bmatrix} -\frac{1}{2}\ (\lambda + 3) & \frac{1}{2}\ (1-\lambda) \\ \frac{9}{10}\ (1+\lambda) & -\frac{1}{10}\ (11 - 9\lambda) \end{bmatrix} \tag{S4}$$

The stability of the 2D system can be determined from the trace-determinant plane (Strogatz, 2018). The determinant of the Jacobian is $\Delta = \frac{1}{5}\ (6 - 4\lambda)$ and the trace is $\tau = \frac{1}{5}\ (-13 + 2\lambda)$. The transition bias is always $-1 < \lambda < 1$, hence $\Delta > 0$, $\tau < 0$, and $\tau^2 - 4\Delta > 0$, thus the coexistence equilibrium is a stable fixed point.

5.2.2 Three phenotypes $N = 3$

The following differential equations describe the system with three phenotypes where $M = \sum_{i=1}^{N} x_i$.

$$\begin{aligned}
\frac{dx_1}{dt} &= r_1\ x_1 \left(1 - \frac{M}{K}\right) + c\ r_1\ \ [(1-\lambda)\ x_2 - (1+\lambda)\ x_1)] \\
\frac{dx_2}{dt} &= r_2\ x_2 \left(1 - \frac{M}{K}\right) + c\ r_1\,[(1+\lambda)\ x_1 + (1-\lambda)\ x_3 - 2x_2)] \\
\frac{dx_3}{dt} &= r_3\ x_3 \left(1 - \frac{M}{K}\right) + c\ r_1\ \ [(1+\lambda)\ x_2 - (1-\lambda)\ x_3)]
\end{aligned} \tag{S5}$$

The Jacobian of the system at a point (x_1, x_2, x_3) is

$$J = \begin{bmatrix} r_1\ (1-\frac{M}{K}) - r_1\ \frac{x_1}{K} - c\ (1+\lambda)\ r_1 & c\ (1-\lambda)\ r_1 - r_1\ \frac{x_1}{K} & -r_1\ \frac{x_1}{K} \\ c\ (1+\lambda)\ r_1 - r_2\frac{x_2}{K} & r_2(1-\frac{M}{K}) - r_2\frac{x_2}{K} - c\ r_1 & c\ (1-\lambda)\ r_1 - r_2\frac{x_2}{K} \\ -r_3\frac{x_3}{K} & c\ (1+\lambda)\ r_1 - r_3\frac{x_3}{K} & r_3(1-\frac{M}{K}) - r_3\frac{x_3}{K} - c\ (1-\lambda)\ r \end{bmatrix} \tag{S6}$$

Using the coexistence equilibrium, $(x_1^*, x_2^*, x_3^*) = K(3+\lambda^2)^{-1}((1-\lambda)^2, (1-\lambda)(1+\lambda), (1+\lambda)^2)$ with $r_2 = \frac{3}{5}r_1$, and $r_3 = \frac{1}{5}r_1$, we obtain eigenvalues $-\frac{3\lambda^2-8\lambda+9}{5(\lambda^2+3)}r_1$, $-c\ (2+\sqrt{1-\lambda^2})r_1$ and $-c(2-\sqrt{1-\lambda^2})r_1$. The range of polynomials in λ in the first eigenvalue are positive for $-1 < \lambda < 1$, shown later in this section. Since $-1 < \lambda < 1$, $\sqrt{1-\lambda^2}$ is real-valued. Thus, again, growth rate r_1 and transition speed c cannot affect the stability of the system with three phenotypes, $N = 3$. For simplicity, we continue with $r_1 = 1$, and $c = 1$ to get

$$J^* = \begin{bmatrix} -\frac{\lambda^3+2\lambda^2+\lambda+4}{\lambda^2+3} & -\frac{\lambda^3+\lambda-2}{\lambda^2+3} & -\frac{(\lambda-1)^2}{\lambda^2+3} \\ \frac{1}{5}(\lambda+1)\left(5+\frac{3(\lambda-1)}{\lambda^2+3}\right) & -\frac{7\lambda^2+33}{5(\lambda^2+3)} & \frac{1}{5}(1-\lambda)\left(5-\frac{3(\lambda+1)}{\lambda^2+3}\right) \\ -\frac{(\lambda+1)^2}{5(\lambda^2+3)} & -\frac{(\lambda+1)^2}{5(\lambda^2+3)}+\lambda+1 & \frac{5\lambda^3-6\lambda^2+13\lambda-16}{5(\lambda^2+3)} \end{bmatrix} \tag{S7}$$

The characteristic polynomial of the Jacobian is a 3rd order polynomial of the form $P(x) = x^3 + a_2x^2 + a_1x + a_0$ where

$$\begin{aligned}
a_2 &= \frac{5\lambda^4 + 42\lambda^2 - 32\lambda + 81}{(\lambda^2+3)\,(3\lambda^2 - 8\lambda + 9)} = \frac{P_4(\lambda)}{P_1(\lambda)\ P_2(\lambda)} \\
a_1 &= \frac{23\lambda^2 - 8\lambda + 69}{(\lambda^2+3)\,(3\lambda^2 - 8\lambda + 9)} = \frac{P_3(\lambda)}{P_1(\lambda)\ P_2(\lambda)} \\
a_0 &= \frac{5}{3\lambda^2 - 8\lambda + 9} = \frac{5}{P_2(\lambda)}
\end{aligned}$$

Now, according to the Routh-Hurwitz stability criterion (Gantmacher, 2009), the system is stable if and only if a_2, a_1, and a_0 are positive and $a_2\ a_1 - a_0 > 0$.

Above, we have defined four polynomials in λ. To show that a_2, a_1, and a_0 are positive, we determine the positivity of each polynomial. $P_1(\lambda)$ is always positive for any real transition bias.

The derivative of $P_2(\lambda) = 3\lambda^2 - 8\lambda + 9$ is $6\lambda - 8$ and vanishes at $\lambda = \frac{4}{3}$. As $P_2(\lambda)$ is a parabola opening upwards, $P_2(\frac{4}{3}) = \frac{11}{3}$ is a minimum. Thus, $P_2(\lambda)$ is positive for a transition bias $-1 < \lambda < 1$.

The derivative of $P_3(\lambda) = 23\lambda^2 - 8\lambda + 69$ is $46\lambda - 8$ and vanishes at $\lambda = \frac{4}{23}$. As also $P_3(\lambda)$ is a parabola opening upwards, $P_3(\frac{4}{23}) = \frac{1571}{23}$ is a minimum. Thus, also $P_3(\lambda)$ is positive for a transition bias $-1 < \lambda < 1$.

The first derivative of $P_4(\lambda) = 5\lambda^4 + 42\lambda^2 - 32\lambda + 81$ is $20\lambda^3 + 84\lambda - 32$ and vanishes at $\lambda^* \approx 0.37$. The second derivative of $P_4(\lambda)$ is $60\lambda^2 + 84$ which is always positive for real λ. Thus, $P_4(\lambda^*) \approx 75$ is a minimum as the curvature is always positive. Thus, $P_4(\lambda)$ is positive for a transition bias $-1 < \lambda < 1$.

Therefore, a_2, a_1, and a_0 are positive for a transition bias $-1 < \lambda < 1$. Finally, we need $a_2\ a_1 - a_0 > 0$ to show that all eigenvalues of the Jacobian have a negative real part.

$$a_2\ a_1 - a_0 = \frac{4\left(25\lambda^6 + 294\lambda^4 - 208\lambda^3 + 1153\lambda^2 - 624\lambda + 1296\right)}{\left(\lambda^2+3\right)^2\left(3\lambda^2 - 8\lambda + 9\right)^2} = 4\frac{P_5(\lambda)}{P_1^2(\lambda)P_2^2(2)}$$

Following a similar procedure as above reveals that $P_5(\lambda)$ is positive for transition bias $-1 < \lambda < 1$. Thus, all Routh-Hurwitz conditions are satisfied, and the coexistence equilibrium is a stable fixed point.

5.2.3 $N > 3$ phenotypes

We wrote a Mathematica script (Wolfram Research, 2020) that computes the eigenvalues for any number of phenotypes N and plots them for the range of the transition bias $-1 < \lambda < 1$. As an example, Fig. S3 shows the eigenvalues for $N = 7$, which are all negative for realistic ranges of our model parameters. We thus conclude that the coexistence phenotype distribution Eq. (2) is stable for all N. The script is available at DOI: 10.5281/zenodo.7294563.

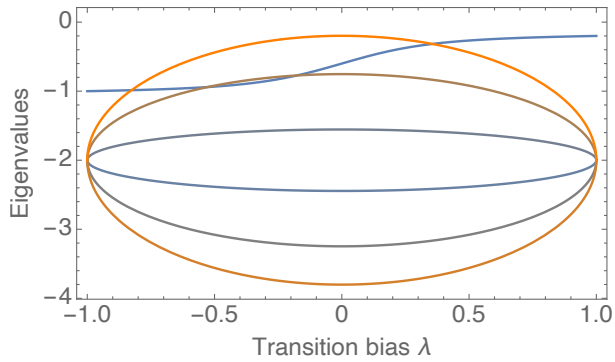

Figure S3: **The coexistence phenotype distribution is locally stable for any number of phenotypes**. The Jacobian matrix of the system Eq. (1) is evaluated at the coexistence phenotype distribution, $x_i^* = K\frac{(1-\lambda)^{N-i}\ (1+\lambda)^{i-1}}{\sum_{j=1}^{N}(1-\lambda)^{N-j}\ (1+\lambda)^{j-1}}$, with $r_1 = 1$, $c = 1$. For the number of phenotypes $N = 7$, all 7 eigenvalues of the Jacobian matrix at the coexistence phenotype distribution are negative. Thus, the coexistence phenotype distribution is locally stable.

5.3 Model extensions

5.3.1 Unequal competition

In the original model, we assumed that all phenotypes share the resources identically. However, resource utilization of phenotypes may differ and lead to a different competitiveness of phenotypes. To account for this aspect, here we extend the model by including phenotype-specific competition coefficients α_i. We assume that mesenchymal-like cells use fewer resources than epithelial-like cells and that competition coefficients decrease similarly to growth rates. This assumption incorporates a classical r-K trade-off into our model with more proliferative but less competitive epithelial cells and less proliferative but more competitive mesenchymal cells (Pianka, 1970). Rescaling the competition coefficients then gives $\alpha_i = r_i \cdot (1\ \textit{time unit})$ for the ith phenotype. Thus, we replace M in Eqs. (1) with $\tilde{M} = \sum_{i=1}^{N} \alpha_i\ x_i$ and obtain for the untreated dynamics

$$\begin{aligned}
\frac{dx_1}{dt} &= r_1\ x_1 \left(1 - \frac{\tilde{M}}{K}\right) + c\ r_1\left[(1-\lambda)\ x_2 - (1+\lambda)\ x_1)\right] \\
&\vdots \\
\frac{dx_i}{dt} &= r_i\ x_i \left(1 - \frac{\tilde{M}}{K}\right) + c\ r_1\left[(1+\lambda)\ x_{i-1} + (1-\lambda)\ x_{i+1} - 2\ x_i)\right] \\
&\vdots \\
\frac{dx_N}{dt} &= r_N\ x_N \left(1 - \frac{\tilde{M}}{K}\right) + c\ r_1\left[(1+\lambda)\ x_{N-1} - (1-\lambda)\ x_N)\right]
\end{aligned} \tag{S8}$$

This set of equations has a saddle point and a stable equilibrium similar to the original model. The state with no cells is a saddle-node equilibrium, i.e., unstable. The stable equilibrium is given by $x_i^* = K \frac{(1-\lambda)^{N-i}\ (1+\lambda)^{i-1}}{\sum_{j=1}^{N}\ \alpha_j\ (1-\lambda)^{N-j}\ (1+\lambda)^{j-1}}$. As the competition coefficients α_j only appear in the denominator they only affect the normalization factor, e.g. $\Pr(i \mid \lambda, N) = \frac{x_i^*}{\sum_{j=1}^{N}\ x_j*} = \frac{\sum_{j=1}^{N}\ \alpha_j\ (1-\lambda)^{N-j}\ (1+\lambda)^{j-1}}{K\ \sum_{j=1}^{N}\ (1-\lambda)^{N-j}\ (1+\lambda)^{j-1}}\ x_i^*$. The normalization does not affect the stable phenotype distribution and the transition bias λ still solely determines the stable phenotype distribution. Notably, now the abundances, particularly of the mesenchymal phenotype, can exceed the carrying capacity K up to an effective carrying capacity given by $\tilde{K} = \frac{K\ \sum_{j=1}^{N}\ (1-\lambda)^{N-j}\ (1+\lambda)^{j-1}}{\sum_{j=1}^{N}\ \alpha_j\ (1-\lambda)^{N-j}\ (1+\lambda)^{j-1}}$ (Fig. S4). This higher abundance of less proliferative but more competitive mesenchymal phenotypes increases the treatment efficiencies for intermediate and high transition biases (Fig. S5).

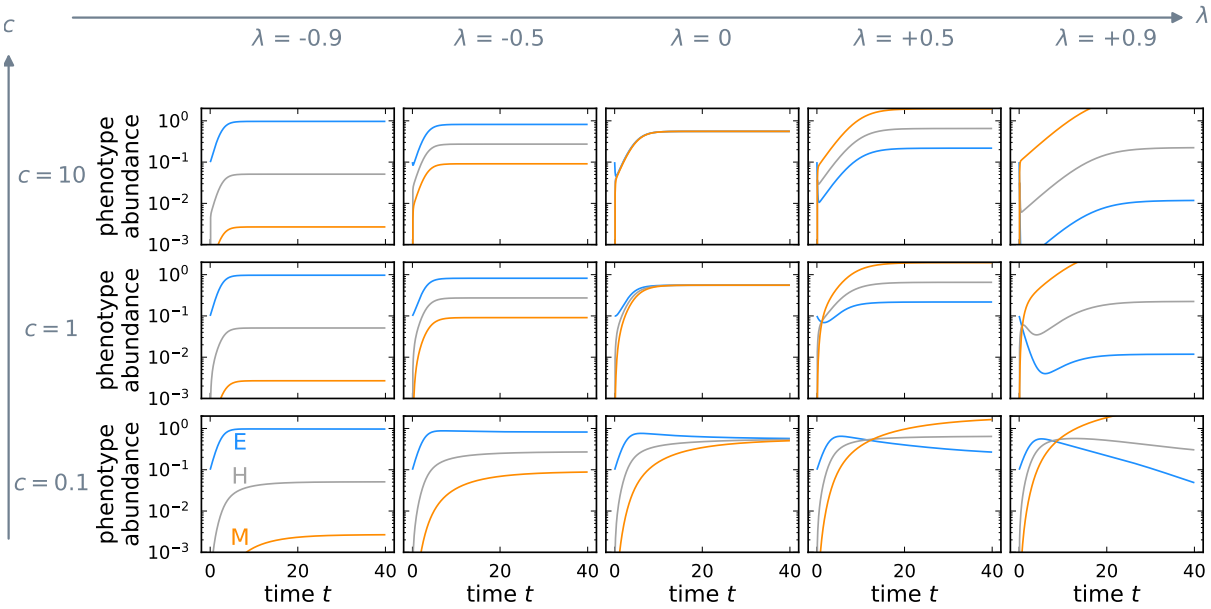

Figure S4: **Unequal competition allows tumor burdens higher than the carrying capacity**. The panels show the simulated equilibration dynamics of tumor phenotypes from the same initial condition, $(x_1, x_2, x_3) = (\frac{1}{10}, 0, 0)$, for different combinations of transition speed c and transition bias λ. We assume that cells consume resources proportional to their growth rate, $\alpha_i = r_i \cdot (1\ \textit{time unit})$. Since mesenchymal cells consume fewer resources, the higher the mesenchymal proportion, the more cells can be sustained above the carrying capacity.

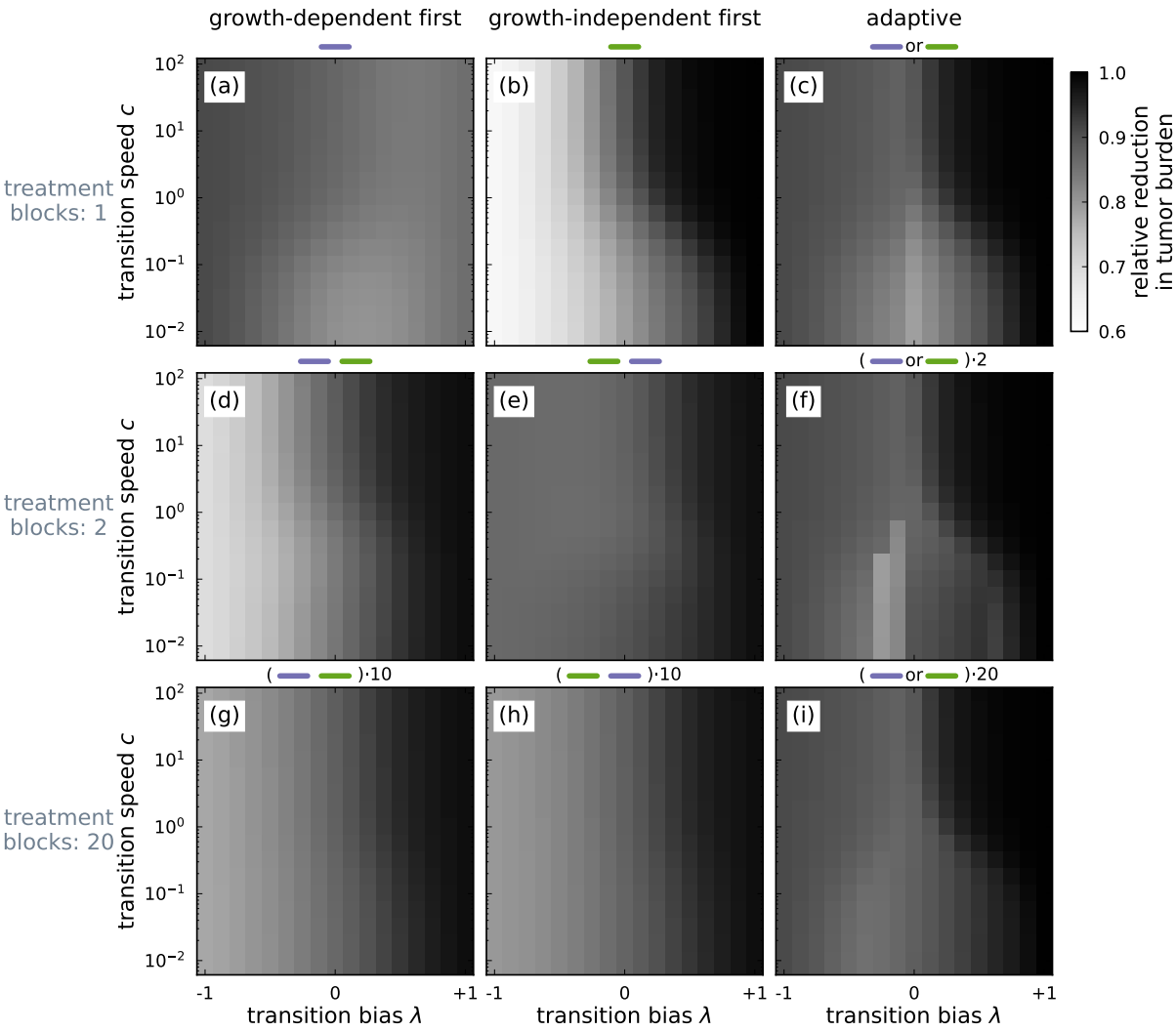

Figure S5: **Unequal competition improves treatment efficiencies for unbiased and mesenchymal-biased tumors**. The heatmap shows the relative reduction in tumor burden from the abundance fixed point $\frac{\sum_{i=1}^{3} x_i - \tilde{K}}{\tilde{K}}$ at the stable phenotype distribution for unequal competition where $\tilde{K} = \frac{K \sum_{j=1}^{3} (1-\lambda)^{3-j} (1+\lambda)^{j-1}}{\sum_{j=1}^{3} \alpha_j (1-\lambda)^{3-j} (1+\lambda)^{j-1}}$. The intensity of growth-independent treatment is $m_I \approx 0.65$. Darker colors represent a higher reduction and, thus, a better outcome. We evaluate the effect of splitting the treatment period into multiple treatment blocks (rows) and investigate different treatment schemes with either predefined or adaptive treatment sequences (columns).

5.3.2 Phenotype-dependent transition speed

Here, we investigate the effect of using $c\ r_i$ for the transition speed of phenotype i instead of $c\ r_1$, i.e., phenotypic transitions are coupled to cell divisions, and the transition rates are scaled by the growth rate of each phenotype.

$$\begin{aligned}
\frac{dx_1}{dt} &= r_1\ x_1 \left(1 - \frac{M}{K}\right) + c\ \left[r_2\ (1-\lambda)\ x_2 - r_1\ (1+\lambda)\ x_1)\right] \\
&\vdots \\
\frac{dx_i}{dt} &= r_i\ x_i \left(1 - \frac{M}{K}\right) + c\ \left[r_{i-1}\ (1+\lambda)\ x_{i-1} + r_{i+1}\ (1-\lambda)\ x_{i+1} - 2\ r_i\ x_i)\right] \\
&\vdots \\
\frac{dx_N}{dt} &= r_N\ x_N \left(1 - \frac{M}{K}\right) + c\ \left[r_{N-1}\ (1+\lambda)\ x_{N-1} - r_N\ (1-\lambda)\ x_N)\right]
\end{aligned} \tag{S9}$$

This set of equations has two equilibria similar to the original model. One equilibrium is a saddle-node equilibrium of extinction, and the other is a stable equilibrium with a fixed phenotype distribution. This stable equilibrium is given by $x_i^* = K \frac{r_1}{r_i} \frac{(1-\lambda)^{N-i}\ (1+\lambda)^{i-1}}{\sum_{j=1}^{N} \frac{r_1}{r_j}\ (1-\lambda)^{N-j}\ (1+\lambda)^{j-1}}$. The model dynamics with phenotype-dependent transition speed are qualitatively similar to the original model. In this case, however, the stable phenotype distribution depends on the phenotype growth rate, increasing the fraction of more mesenchymal phenotypes (Fig. S6). This leads to stable phenotype distributions with negative skewness for a larger transition bias range (Fig. S7) and an efficiency loss of purely growth-dependent treatment (Fig. S8).

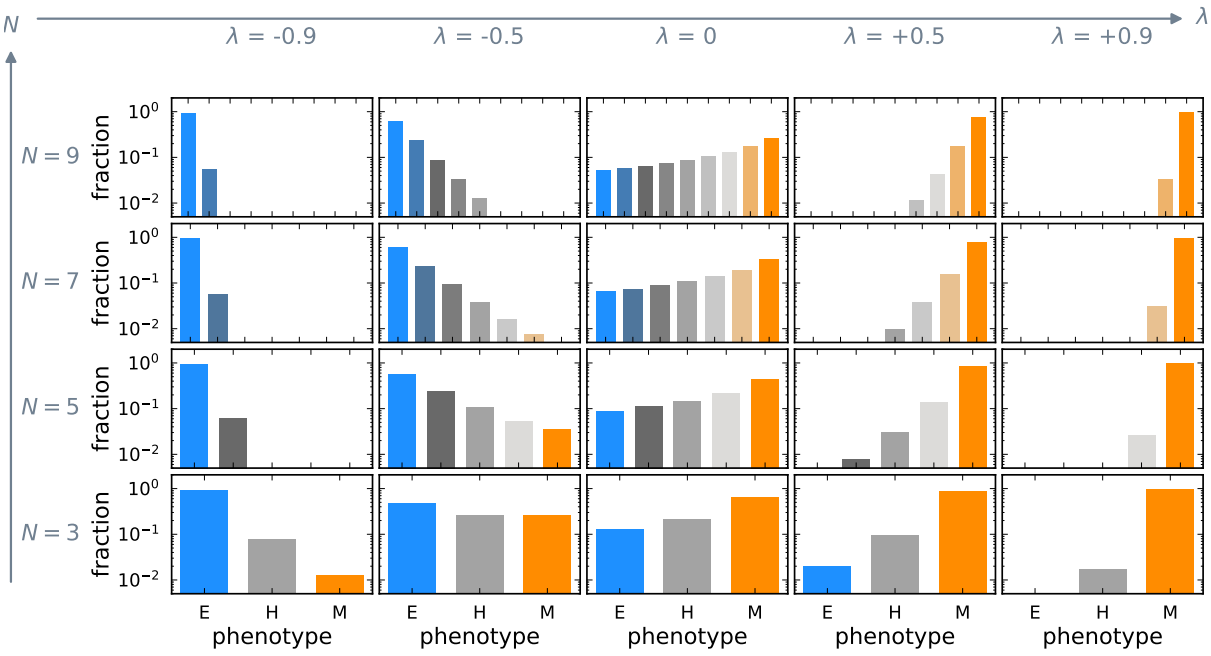

Figure S6: **Phenotype-dependent transition speed does not qualitatively affect the stable phenotype distribution**. Each panel shows the equilibrium distribution of phenotypes for a fixed value of the transition bias and the number of phenotypes. The stable phenotype distribution changes with the transition bias λ. When there is no transition bias to switch to either an epithelial or a mesenchymal-like phenotype, i.e., $\lambda = 0$, the stable distribution is not uniform as faster proliferating cells transition faster. Transition bias towards the epithelial-like phenotype, $\lambda < 0$, leads to an increase in epithelial cells. Conversely, a transition bias towards mesenchymal-like phenotypes, $\lambda > 0$, leads to an increase in mesenchymal cells.

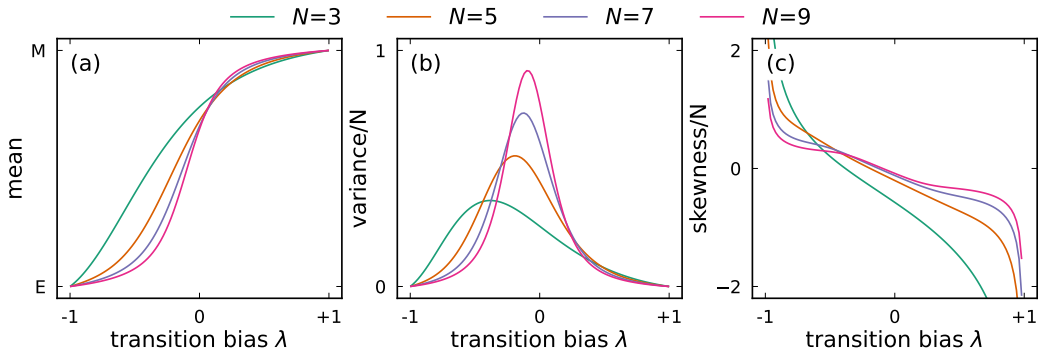

Figure S7: **Phenotype-dependent transition speed decreases the abundance of epithelial phenotypes**. Including phenotype-dependent transition speed breaks the symmetry of the stable phenotype distribution. The overall mesenchymal proportion increases as fast-proliferating epithelial cells transition faster into mesenchymal cells. Thus, the growth-dependent treatment type loses efficiency due to a worse phenotype match for a tumor with phenotype-dependent transition speed.

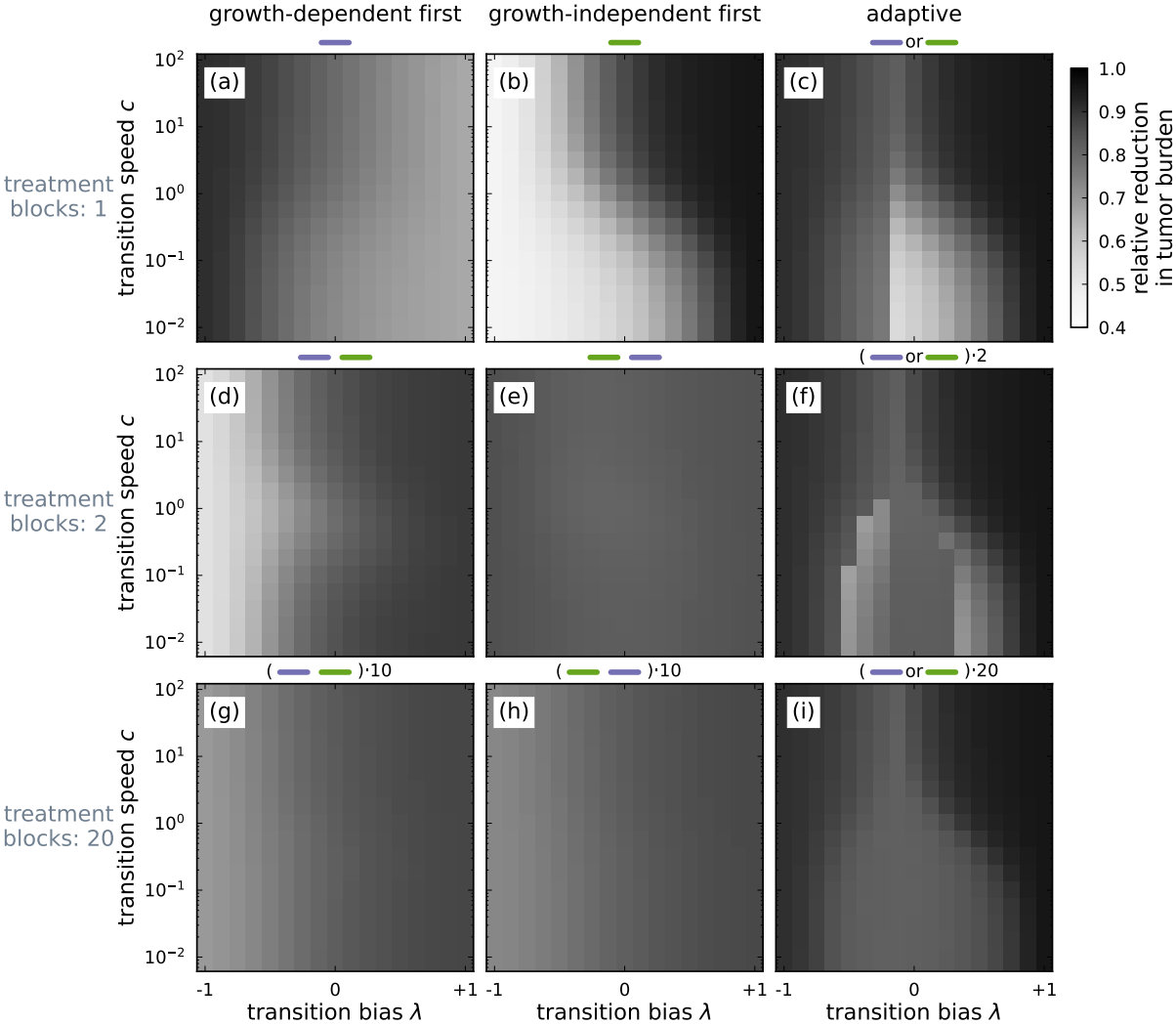

Figure S8: **Phenotype-dependent transition speed improves the treatment efficiency**. The heatmap shows the relative reduction in tumor burden from the abundance fixed point $\frac{\sum_{i=1}^{3} x_i - K}{K}$ at the stable phenotype distribution for phenotype-dependent transition speed. The intensity of growth-independent treatment is $m_I \approx 0.50$. Darker colors represent a higher reduction and, thus, a better outcome. We evaluate the effect of splitting the treatment period into multiple treatment blocks (rows) and investigate different treatment schemes with either predefined or adaptive treatment sequences (columns). The negative effect of transition speed is amplified by phenotype-dependent transition speed. Thus, the overall growth rate of the tumor is decreased, further reducing the tumor burden at the end of the treatment duration.